THERMAL CHARGE NOISE OF A NEAR-SURFACE NITROGEN VACANCY CENTER DIAMOND WITH A PROTECTIVE LAYER

by

Philip C. Chrostoski

A THESIS

Submitted in partial fulfillment of the requirements for the degree of

Master of Science in Physics Graduate Program

of Delaware State University

DOVER, DELAWARE

May 2018

This thesis is approved by the following members of the Final Oral Review Committee:

Dr. Deborah Santamore, Committee Chairperson, Department of Physics and Engineering, Delaware State University

Dr. Essaid Zerrad, Committee Member, Department of Physics and Engineering, Delaware State University

Dr. Gour Pati, Committee Member, Department of Physics and Engineering, Delaware State University

Dr. Marwan Rasamny, External Committee Member, Department of Computer and i Science, Delaware State University

Copyright 2018

By

Philip C. Chrostoski

Dedication

I dedicate this thesis to my parents, Jean and Bill Chrostoski, my fiancée, Olivia Welby, and my brother, Eric Chrostoski, for their love and support throughout my graduate work at Delaware State University.

Acknowledgements

I would first like to thank my undergraduate professors at Southern Illinois University – Edwardsville for their teachings and advise. Without the great background obtained from the enthusiastic professors at SIU-E, I would not have the insight and intuition that I do today. I will always continue to give acknowledgement to my time there at SIU-E, as it is basis for all my scientific work going forward. I would also like to acknowledge my professors at Delaware State University. Their teachings have allowed me to build my intuition and insight into the wonderful world of physics.

I also would like to give a big thank you, and acknowledgement to my research adviser, Dr. Deborah Santamore. The work done under the mentorship of Deborah has given me amazing insight and motivation to continue my journey through my career in physics. I know the work done with her will help me become a prominent member of the physics community. Her mentorship and advise will never be forgotten, and I hope to continue to collaborate and tackle the many mysteries of the universe with her throughout my physics career.

I cannot go without acknowledging my family, friends, and loving fiancée. Without their support I would not have made it this far. I would also like to acknowledge a fellow collaborator, Dr. Pauli Kehayias from the Walsworth group at Harvard, for his helpful insights on my thesis research.

Thermal Charge Noise of a Near-Surface Nitrogen Vacancy Center Diamond with a Protective Layer

Philip Chrostoski

Thesis Adviser: Dr. Deborah Santamore

ABSTRACT

A nitrogen vacancy center in diamond has become an interesting topic to investigate with their applications in magnetic field sensors and quantum computing. A major problem in their applications has been the large amounts of noise. Fluctuations in both the electric and magnetic fields give rise to this noise. At room temperature, the electric field has shown to be the largest factor in the noise. We decided to investigate these thermal fluctuations caused by the electric field. The model used is a system consisting of the NV-center with a protective layer on the surface. We examined different surface materials such as; D-glycerol, propylene carbonate, and others to compare with recent experimental data. The fluctuation dissipation theorem was used to obtain the charge noise spectral density. The noise for the liquid protective layers is less than the solid protective layers initially. The liquids show better noise reduction due to their faster relaxation times for their dipole interactions. Both the real and imaginary parts of the permittivity play key roles in effecting the noise of the system.

Table of Contents

List of Figures and Tables

CHAPTER 1

NITROGEN VACANCY DIAMONDS

1.1 Nanodiamonds:

Diamonds have always been interesting to investigate with their lattice structure formation of carbon. The crystal lattice of the diamonds forms a face-centered cubic (Fig. 1) which packs the atoms as tightly together as possible. This tight packing makes the diamonds lattice very rigid and strong covalent bonding between the atoms. Research had found that with this structure came the highest thermal conductivity for any bulk material above 100 Kelvin (K) [1]. Diamonds have two different types, with two sub types each. There are type Ia, Ib, IIa, and IIb. The type Ia,b diamonds have nitrogen impurities, where the type IIa is highly pure carbon and IIb has boron impurities. During the 1960's, type Ib diamonds were starting to be investigated. Type Ib diamonds make up roughly 0.1% of naturally formed diamonds. The type 1b diamond has isolated nitrogen atoms throughout the crystalline structure. Amid the study of these type Ib diamonds, soviet scientist discovered nanoparticles of diamonds can be formed in nuclear explosions. With this discovery, research into more practical synthesis methods of nanodiamonds began [3]. Years of research allowed for methods such as, ion bombardment, electrochemical synthesis, and laser bombardment to be developed.

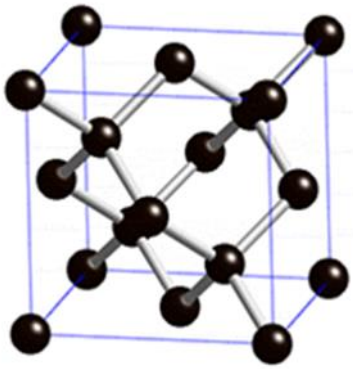

Fig 1: Diamond Crystal Lattice (H.K.D.H Bhadeshia et. al.)

When thinking about a nanodiamond, there are three major aspects to consider for the overall structure; the overall shape, the core, and the surface. At the core of nanodiamonds, there lies a diamond cage which comprises mainly of the carbon atoms [4]. The overall structure has been shown to be both spherical and elliptical. Though the core is very much like bulk diamond, the outer portion of the diamond nanoparticles structure is very much like graphite. The similarity with graphite makes the nanodiamonds more stable than normal diamond. Studies into these nanodiamonds have shown that different defects form within the structure. One very interesting defect is the nitrogen vacancy discovered by nitrogen-15 nuclear magnetic resonance research.

1.2 Nitrogen Vacancy Centers

The nitrogen vacancy (NV) center in a diamond crystal lattice structure is one of many point defects. Defects in diamond are common, arising from irregularities and impurities. These defects have many different effects on the diamond, the most prominent being their color and electric conductivity. The structure of this defect in the lattice is the interchanging of a nitrogen atom with one of the carbon atoms and leaving a vacancy in its nearest neighbor.

This leads to two possible overall charge states; an overall neutral charge or an overall negative charge. Nitrogen has five valance electrons with three of these electrons covalently bonding to the carbon atoms while two remain as lone pairs. The vacancy neighbor will have three unpaired valence electrons from the carbon. Two of them will make a quasi-covalent bond, leaving the last electron unpaired.

The overall symmetry of the lattice is axial with the three unpaired valence electrons constantly changing roles. The neutral state ($N\text{-}V^0$) is paramagnetic and has the one unpaired electron. The neutral state avoided electron paramagnetic detection (EPR) for years. It wasn't until 2008 that EPR in the neutral state was detected. This state avoided detection as the EPR signals are not produced unless there is optical excitation [5]. The $N\text{-}V^0$ ground state signals are too broad, optically exciting them their spin states change, and a better signal was detected. For the negatively charged state ($N\text{-}V^-$) there is an extra electron located in the vacancy. This extra electron gives the system a spin S = 1 pair with one of the three valence vacancy electrons.

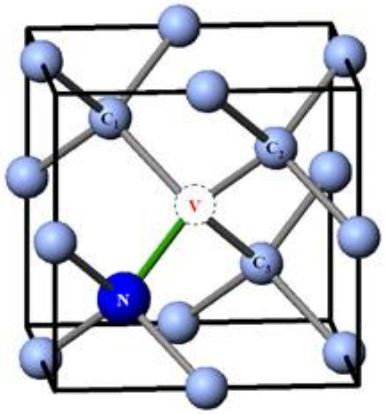

Fig 2: NV Center Lattice (D. D. Awschalom et. al.)

The energy levels (Fig 3) for the NV center have been determined through earlier work in optical, electron paramagnetic resonance, and other theoretical results [6-9]. The techniques used to gain these energy levels were the linear combination of atomic orbitals (LCAO) and group theory. LCAO is a technique which has the electron configuration be represented as wavefunctions. Group theory brought in the symmetry of the diamond, which allowed for the determining of the symmetry of the NV center itself. The superscripts for the energy levels are the resulting allowed m_s spin multiplicity, or spin states. These values of the spin multiplicity range from -S to S which will give a total of 2S+1 allowable spin multiplicities. For example, if S = 1 then m_s can be -1, 0, or 1.

In the absence of an external magnetic field, the ground state for the NV is split. This splitting is due to the magnetic interaction between two of the unpaired electrons. There will be a higher energy when the spins are parallel ($m_s = \pm 1$) and lower when they are antiparallel ($m_s = 0$). The parallel spin states have a higher energy due to quadrupole coupling nuclear mixing of the hyperfine states [10]. These hyperfine states, or structures, form due to the change of the nuclear electric quadrupole moment due to the electric field gradient and the nuclear magnetic dipole moments interaction with the magnetic field generated by the electrons. In the excited state, there is a smaller splitting of the energy level due to smaller interaction energy ($\mathbf{D} \sim 1/r^3$) from a larger separation between the electrons.

Applying an external magnetic field to the $N\text{-}V^-$, will not affect the antiparallel ground state but split the parallel ground state. The antiparallel state will not split due to all its electrons being paired and its overall spin quantum number is S = 0. A strong interaction when the magnetic field is along the defect axis induces a spin-polarization, which will affect the optical absorption and luminescence of the NV center in the antiparallel and negative parallel ground states.

Since electron interaction is mediated by photon interaction and overall spin cannot be changed, optical transitions will have spin conversation and only occur between levels with the same spin. The ^{3}E excited state has an orbital degeneracy which gives rise to spin-orbit interactions. These interactions split the energy level and can be modulated by applying an external static electric field.

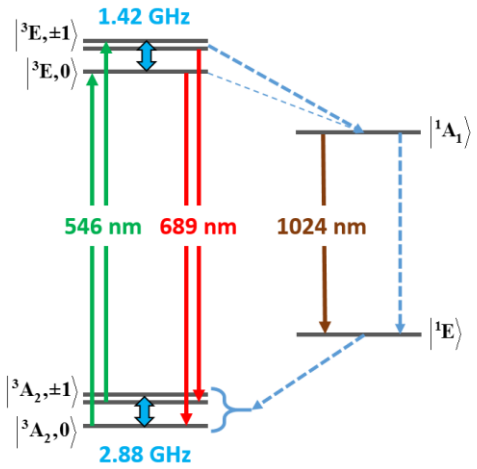

Fig 3. Energy Level Diagram (L. J. Rodgers et. al.)

Modern applications of magnetic field sensors and computing use electric signals to send information. For electric signals, a bit of information can have two states 1 or 0. Quantum information also have two states of information. These states could be energy and time, or position and momentum. These states can be in what are called coherent states. Coherent states are states of "minimum uncertainty" wave packets. The minimum coherent state will have one free parameter that will have its position and momentum dispersion equal small. With minimum uncertainty for our free parameter, we have a very precise knowledge of the free parameter. Coherence of states will give the same phase difference, frequency, and waveform.

Naturally, these coherent states have a time dependence, and the time of these coherent states have been widely investigated [11-13]. These pieces of quantum information are two level quantum mechanical systems which are more widely known as qubits [12].

The difference between the two states of a bit and the two states of a qubit, is a qubit can hold more information in its two coherent states. Instead of just having 1 or 0 for the information in the qubit, the qubit is in a superposition of these values. Being in a superposition of the two states, a correlation between the two states is present unlike with the normal bit. With the qubit being a superposition, we can picture the qubit as a sphere on the real and imaginary axis. This sphere is known as the Bloch sphere. The Bloch sphere is the geometrical representation of the pure state space of these two-level quantum mechanical systems. If you had a few hundred qubits, it would take more bits than there are atoms in the universe to fill up that information.

Along with interactions with electric and magnetic fields, the NV center also has different interactions with stress [14-27]. The NV center has also shown different entanglement effects, such as photon-electron and electron-electron making it more interesting to study [28-33]. These different interactions have been of important study. Investigations into coherent interactions have shown the NV center has very useful applications in magnet field sensors, quantum computing, and frequency-modulated radio receiver in extreme conditions. As stated before, coherence is when two quantum states have the same phase difference, frequency, and waveform. Having this precise knowledge of the system is important as it describes correlations between all physical quantities for single waves up to wave packets. Other studies and materials have been used to investigate these different types of applications, but what makes the NV center interesting is its usefulness at room temperature.

Coherent interactions for many materials require temperatures well below room temperature. Experiments have shown that the NV center diamond has long coherence times for temperatures ranging well above room temperature [34]. Room temperature use has an advantage as it doesn't require large amounts of cooling which can be expensive. This change to quantum information would allow for many applications that would make modern computing and information systems be obsolete.

1.3 Thermal Noise

Working with the NV center quantum coherence, has shown long coherence times when moving the defect near the surface. Having the NV center near to the surface, a few microns deep, allows for greater manipulation of the coherent states. Even with these long quantum coherence times ranging around several milliseconds when near the surface, noise has become a major issue. The noise in a near surface NV center system brings decoherence into the system. Decoherence loses that correlation between the states which makes them desirable. Along with the decoherence, the system has losses of information. Many modern applications have shown that magnetic field noise is very prominent in the NV center system. Fluctuations in the magnetic field from the environment have been shown to couple all the elements of the density matrix. These fluctuations then cause decoherence, dephasing, and dissipation. As temperatures reach room temperature, the electric field from thermal interactions cause a much more prominent amount of noise. The thermal noise, which causes decoherence, dephasing, and dissipation, also hinders the detection method for the NV center. Thermal noise is when charge carriers in a material are agitated by thermodynamic fluctuations. Current detection methods use the fluorescence of the NV center. The noise from the magnetic and electric fields will cause fluorescent line-broadening.

Recently, experiments have coated the NV center with materials as protection from surface noise [35-40]. The mechanism that describes this reduction to the surface noise is unknown. We investigated the NV center system with a protective coating to give a solution to that question. With this type of system, we can consider what the noise of the system will be based off what material is being used as the protective coating. This gives a system that depends on two different materials, which will change up the overall noise of the system. The method widely used to determine the thermal noise of a system, is the fluctuation-dissipation theorem. The medium described by the fluctuation-dissipation theorem is characterized by a generalized impedance, or in our case, a generalized susceptibility.

Susceptibility can be described as the change of an extensive property, such as energy, by the variation of an intensive property, such as temperature. We are looking at thermal fluctuations due to the electric field, so our generalized susceptibility will be the systems electric susceptibility. Electric susceptibility is relation how responsive the polarization is to an applied electric field. With this relation, we began by looking at the polarization to determine the generalized susceptibility. The thermal fluctuations that will be described by the fluctuation-dissipation theorem require a correlation between the charges in the system. This required me to use the quantum mechanical version of the polarization. Dissipation in a system is inherently a time dependent process as it is the change of a systems energy. The fluctuation-dissipation theorem will give me the system's thermal charge noise spectrum. Once we have this, we can begin analyzing how different materials will affect the overall noise of the system.

Chapter 2

Current Research of NV Center Diamonds

2.1 Nuclear Magnetic Resonance

In nature, there is a physical phenomenon where nuclei will absorb energy from a magnetic field and re-emit electromagnetic radiation. This re-emission will only occur when the energy is at a resonance frequency. This phenomenon has been named nuclear magnetic resonance (NMR). Observations of NMR allow for the study of many quantum mechanical properties of atomic nuclei. Applications of NMR using a technique known as NMR spectroscopy has allowed for the further investigation of many subjects such as, molecular physics and crystals. NMR spectroscopy uses NMR to gain the information about reaction state, chemical environment of molecules, structure, and dynamics in materials.

To have NMR possible in a material, it must have an intrinsic angular momentum and magnetic moment. In other words, the material must have a non-zero spin. This requirement makes the negative NV center a useful candidate for NMR research. Recent work has investigated NMR phenomena with the negative NV center diamond. The research investigated the magnetic resonance phenomenon by looking at the magnetic field dependence of an ensemble of negative NV center in enriched Carbon-13 (A. Jarmola *et al*) and by using the negative NV center near surface as a small volume NMR spectroscopy sensor (P. Kehayias *et al*).

The optical excitation of the negatively charged NV center diamond causes a spin transfer. This stems from the optical polarization placed on the NV center. This spin transfer is enhanced even further when a strong external magnetic field is present. The highly nuclear-polarized system would give rise to a more sensitive magnetic resonance device. Varying the degree of enrichment of the Carbon-13 system can change its usefulness at room temperature. Understanding the magnetic resonance for the different enrichments leads to new applications in diamond based rotational sensors and fundamental physics research.

To detect the magnetic resonances, confocal microscopy was the technique chosen. The enrichment of the samples ranged from 1.1% - 99.9% Carbon-13. For each sample spectrum, their individual fluorescence intensity, obtained when the microwave frequency was far from the resonance was detuned, were normalized. There data showed a splitting of the ground state energy level due to resonances of their spins. Depending on the sample the peaks are different. In figure 4, the natural abundance of carbon-13 (1.1%) shows a large central peak which is the carbon-13 around the nuclei of the NV center. As the abundance of the carbon-13 rises, the side peaks get larger due to the higher probability of finding the carbon-13 in the first shell.

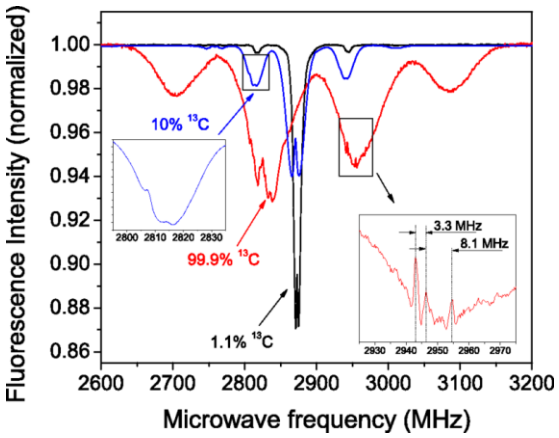

Fig 4. ODMR spectra for natural abundance of Carbon-13 (1.1%) and enriched Carbon-13 (10% and 99.9%) (Jarmola et. al.)

The peaks correspond to the spins of the shells. The natural abundance has the spin for the ground state peak resonate, but the four peaks for the enriched give different spin states of the first shell (-3/2, -1/2, 1/2, 3/2). The importance of this is that the NV center is showing clear nuclear magnetic resonance. Here the resonance is occurring due to optical excitation creating a resonance for different spin states at different frequencies. For this experiment, they also looked at different applied magnetic fields to see how the resonances would change.

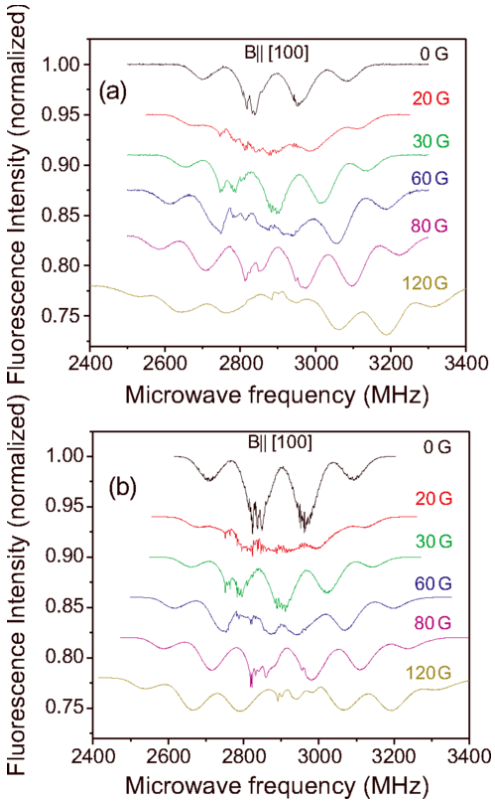

Fig 5. Resonance of NV center for different applied magnetic fields for simulation and experiment (Jarmola et. al.)

Figure 5 shows that as an external magnetic field is applied, the resonance sensitivity is dropping proportionally to the strength of the magnetic field. The relationship between the loss of sensitivity with the external magnetic field shows that magnetic field noise will be an issue for nuclear resonance of the NV center diamond. Solutions for reducing this surface noise have been thought up intuitively by other researchers.

Experiments using a protective layer (Kehayias et. al.) have shown an increase in sensitivity for nuclear magnetic resonance applications of the NV center diamond.

Looking at NMR spectroscopy for negatively charged NV center diamonds, the sensitivity at room temperature is rather low. When placing a protective layer of liquid or thin-films, longer measurement times and sensitivity have been seen. Following this protective layer system, a picolitre of cesium fluoride (CsF) in glycerol and pure glycerol were used with the nanodiamond chip of negatively charged NV center diamonds. Using correlation spectroscopy on hydrogen and fluorine – 19 isotope nuclei, the resonance at the Larmor frequency was detected for each respectively.

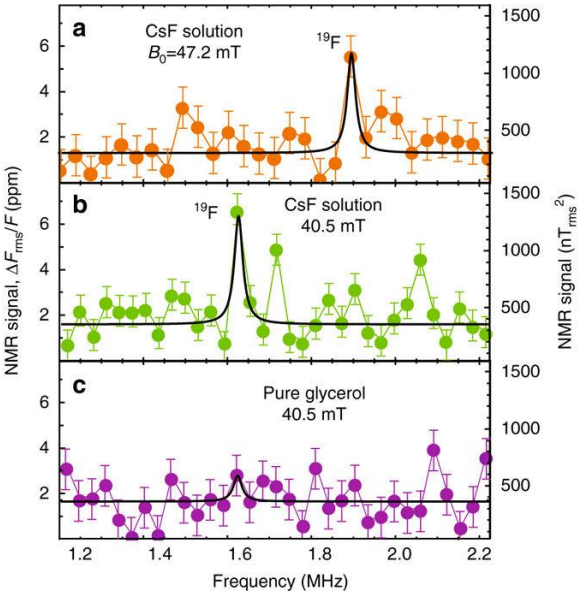

Fig 6. NMR Signal of flourine-19 isotope for CsF in glycerol and pure glycerol (P. Kehayias et. al.)

Figure 6 shows that the CsF system is giving a higher sensitivity to that of pure glycerol. A clear peak of resonance in the fluorine-19 isotope can be seen for the different magnetic field strengths for the CsF solution. The different resonances are from the gyromagnetic properties of floruine-19. Though the sensitivity increases with the protective layer, the signal has substantial noise. This magnetic field noise has been studied, but researchers were wondering if there is more to the room temperature noise than just magnetic noise from external magnetic fields.

2.2 Decoherence Due to Noise

NV center diamonds excel as room temperature quantum sensors, as seen by the previous work. They have long coherent spin states and working near the surface allows for manipulation of the external degrees of freedom. Having the NV center near the surface, the external degrees of freedom can be strongly coupled giving nanoscale spatial resolution in imaging. The major problem is the substantial noise being seen. Magnetic field noise has been a big factor, but the NV center has a magnetic-dipole-forbidden transition. This forbidden transition, due to selection rules, can be used as a probe to other candidates for noise. With the NV center near the surface, environmental interactions are unavoidable at room temperature. Research investigating single quantum (SQ) and double quantum (DQ) relaxation rates was used to probe where the environmental effects were coming from.

SQ and DQ relaxation rates are the rates at which decoherence of the quantum states takes place. When these rates are fast, that means there is a quicker rate of decoherence in the system. Techniques known as SQ and DQ relaxation spectroscopy are used to gain a spectral character of the noise sources. When there is a quantum coherence in a material, a chemical shift can be observed. The quantum coherent states are excited states, so the longer they can stay in these coherent states the longer the chemical shift is observed.

Looking at the ground state Hamiltonian for the NV center, we can see the contributions from the strain, the electric field, and the magnetic field,

$$H_{NV} = \left(hD_{gs} + d_{\parallel}\Pi_{\parallel}\right)S_z^2 + g\mu_B \boldsymbol{B}\cdot\boldsymbol{S} - \frac{d_{\perp}\Pi_{\perp}}{2}(S_+^2 + S_-^2). \quad (1)$$

Here **B** is the magnetic field, **S** is the spin-1 operator, $d_{\parallel,\perp}$ are the dipole moment parallel and perpendicular to the symmetry axis, $\frac{g\mu_B}{h}$ is the gyrometric ratio, D_{gs} is the crystal-field splitting, and $\Pi_{\parallel,\perp}$ are corresponding to the total electric field components ($\boldsymbol{\Pi} = \boldsymbol{E} + \boldsymbol{\sigma}$). These fields will give sources of noise due to the fluctuations caused by the fields as time progresses while in the coherent state.

A major piece of coherent states is their simultaneous phases. Fluctuations due to external fields cause a dephasing effect in the NV center coherent spin state. By exciting the system with CPMG (Carr-Purcell-Meiboom-Gill) pulses at the Larmor frequency ($\omega = -\frac{g\mu_B}{h}B$), the systems echo time can be observed. The observation of the fluorescence as a function of the precession time will give the coherence as a function of the precession time. This was done for both the SQ and DQ relaxation systems.

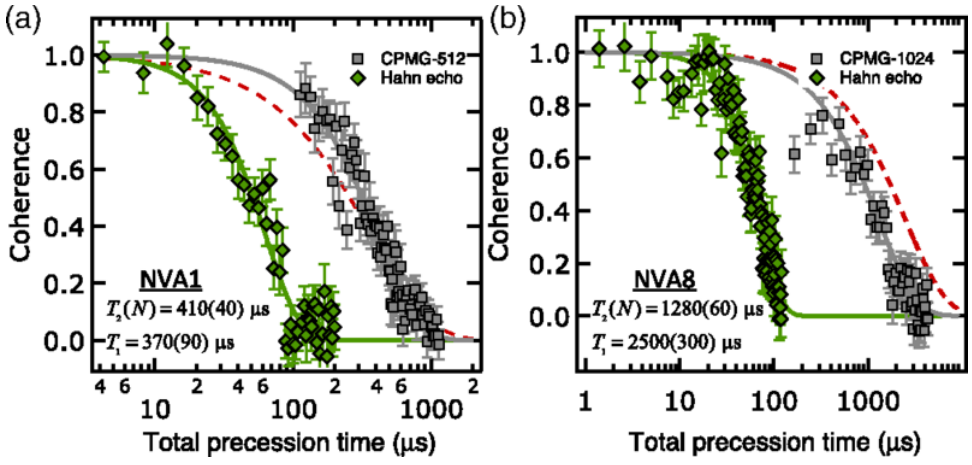

Fig. 7: SQ coherence time at (a) 37.1 MHz and (b) 1376 MHz (B. A. Myers et. al.)

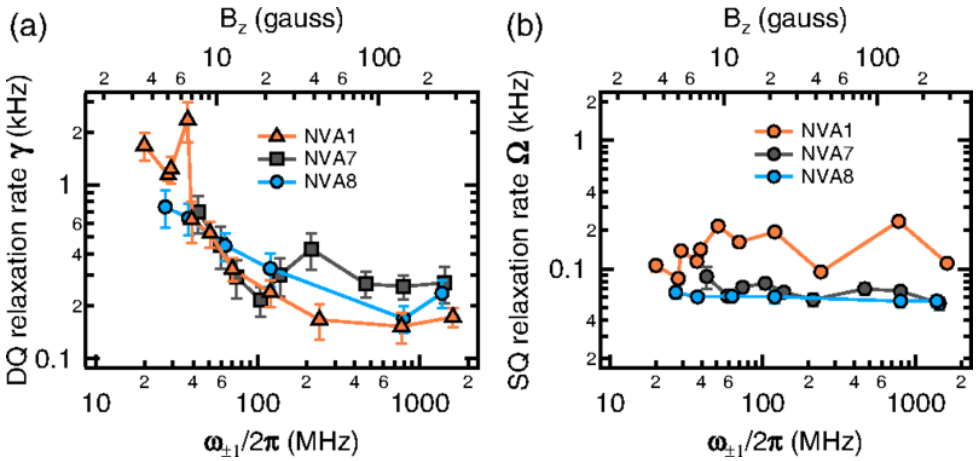

Fig. 8: DQ and SQ Relaxation rate as a function of splitting frequency. (B. A. Meyers et. al.)

Figure 7 shows that a higher frequency will give a longer coherence time, but there is something causing decoherence. Looking at figure 8, the DQ relaxation is highly frequency dependent. Comparing the DQ and SQ relaxation rates for the NV center, insights into the noise sources are gained. The double-quantum relaxation spectroscopy shows that as the external magnetic field tunes the frequency, a $f^{-\alpha}$ dependence appears. This is attributed to surface - related noise from the electric field. The double quantum relaxation is playing a major role in the dephasing of the coherent states no matter the applied magnetic field. The noise spectra gives a clearer insight into the decoherence of the near surface NV centers.

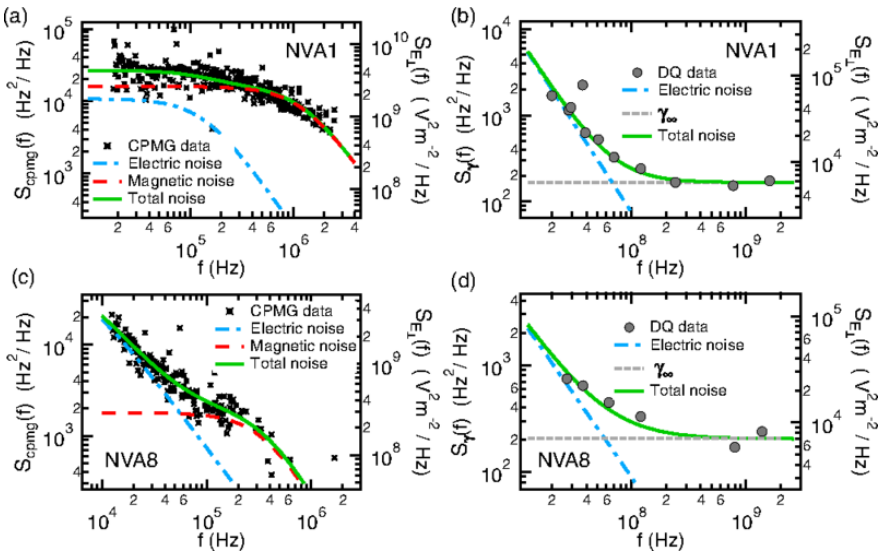

Fig. 9: Measured noise spectra as a function of coupling power (Hz^2/Hz) and transverse electric field power ($V^2m^{-2}/\,Hz$) (B. A. Myers et. al.)

Figure 9 shows a prominent effect of the electric field on the noise spectra for the SQ (a,c) and DQ (b,d) systems. The two data sets are looking at the samples labeled NVA1, which had its NV center at a depth of 150μm, and NVA8 with NV depth of 30μm. Comparing the typical magnetic noise and electric noise with the data fitted to the noise function, there is a difference in total noise, but a similar trend is seen. For the DQ systems, the noise is highly contributed by the electric field noise for both sets of data. The SQ noise fits highly with the magnetic noise for the NVA1 data set, but the NVA8 data set still shows a high dependence on the electric noise near the surface.

The two samples are showing that as the NV center gets nearer to the surface, the interactions with the environment are beginning to come mainly from the electric field. As the near-surface NV centers are being considered for room temperature applications, it is the thermal interactions that the electric field noise is derived. Using a protective layer has shown greater sensitivity, so the surface electric field noise is being reduced by using a protective layer.

2.3 Electric Field Noise with a Protective Layer

With noise a problem for the sensitivity and decoherence for applications of the NV center, protective layers have been investigated for reducing the noise. When using a material as a protective layer, different material characteristics must be considered. The material must not evaporate quickly when in room temperature conditions and any reactions when laying on the surface must happen quickly. The reactions also shouldn't damage the NV center in any way. Protective materials such as polymethyl methacrylate, polyvinylidene fluoride, and microscope immersion oil have been used. Research into other materials, such as d-glycerol and propylene carbonate has been done to see how well they protect the NV center from the surface noise.

Glycerol is an alcohol with hydroxyl groups that can donate protons to the environment. Glycerol also has a high dielectric constant of 42. Propylene carbonate has tightly bound hydrogen atoms giving it an even bigger dielectric constant of 64. The dielectric constant is important as it tells us about how the material will interact with an electric field. A way to notice if the protective layer is helping, is to look at the echo time of the NV center with and without the added material. The echo time is the time for the signal to last after excited by a pulse. When looking at the echo time of the NV center with and without the protective layers, a noticeable rise in the echo time is seen when a protective layer is present.

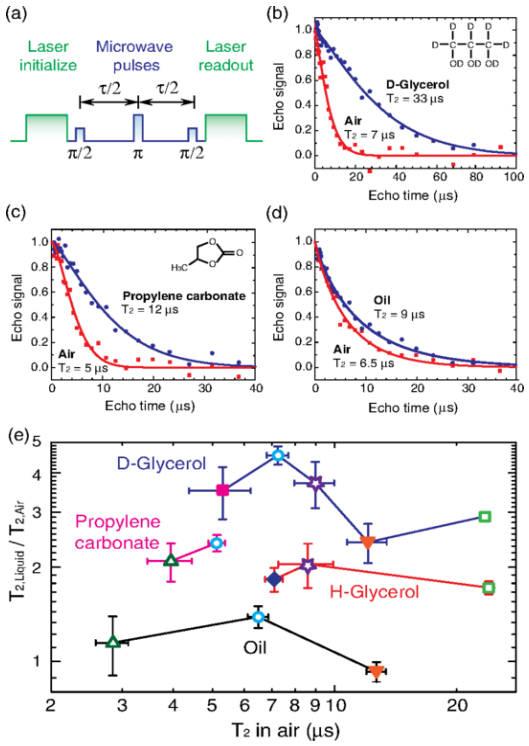

Fig. 10: Comparison of echo time with and without the protective layers added. (M. Kim et. al.)

Fig. 10 shows a 4.6-fold increase in the echo time when d-glycerol was placed on the NV center. Not far behind is propylene carbonate with a 2.4-fold increase in the echo time. The microscope immersion oil, with a dielectric constant of 2.3 showed only a 1.4-fold increase in the echo time. This shows a definite correlation between the materials dielectric constant and the increase in echo time.

Surface electron spins, dark spins, are the usual suspect for surface noise and the loss of coherence. The protective materials could be passivating these dark spins from causing the decoherence. Hitting the NV center with another pulse part way through its echo time will get these dark spins to resonate. Doing this with and without the protective layers can show if the protective layer is indeed passivating the dark spins of the NV center surface.

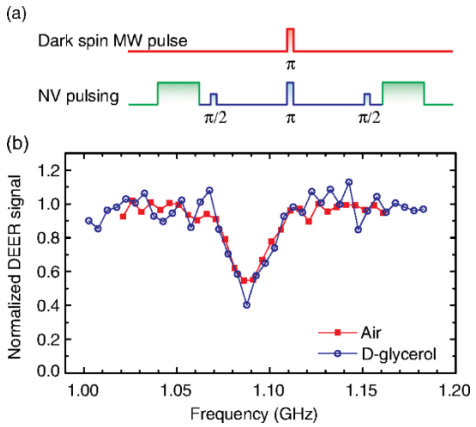

Fig. 11: Double electron-electron signal with and without the d-glycerol protective layer (M. Kim et. al)

Fig. 11 shows no change in the dark spin signal when d-glycerol was added. The dark spins of the NV center are playing a negligible part in the surface noise from the NV center. Considering the dielectric constants of the materials again, the electric field must be the major source in the electric field noise.

If we consider a single charge q at the NV center, the NV center Hamiltonian can help lead to determining the effects of the electric field on the coherence of the NV center. The NV center Hamiltonian will be given by [13],

$$H = (hD + d_{\parallel}E_z)\left[S_z^2 - \frac{2}{3}\right] + \mu_B g_{NV}\boldsymbol{S}\cdot\boldsymbol{B} - d_{\perp}\left[E_x\left(S_xS_y + S_yS_x\right) + E_y\left(S_x^2 - S_y^2\right)\right]. \qquad (2)$$

Here h is Planck's constant, **B** is the applied magnetic field, **S** is the spin-1 operator, $d_{\parallel,\perp}$ are the dipole moment parallel and perpendicular to the symmetry axis, D is the zero-field splitting, μ_B is the Bohr magnetron, and g_{NV} is the NV electron spin g-factor. Assuming the magnetic field to be along the z-axis, solving for the energy eigenvalues for the three magnetic sublevels will give the electric field effect on the NV spin precession frequency.

The precession frequency from the resulting calculation will be [13],

$$\frac{\Delta\omega_{\pm}}{2\pi} = \left(\frac{d_{\parallel}}{h}\right)E_z \pm \frac{1}{2}\frac{\left(\frac{d_{\parallel}}{h}\right)^2 E_{\perp}^2}{\left(\frac{\gamma}{2\pi}\right)B_z}. \qquad (3)$$

Here $E_{\perp}^2 = E_x^2 + E_y^2$, and $\frac{\gamma}{2\pi} = \frac{\mu_B g_{NV}}{h}$. The frequency shift is directly related to the magnitude of the electric field in the z-direction and to the magnitude squared of the perpendicular directions. A large electric field would cause frequency shifts, which in tow would affect the coherence time of the NV center. Spin echo measurements were taken on the system with and without the application of d-glycerol with different pulse amounts.

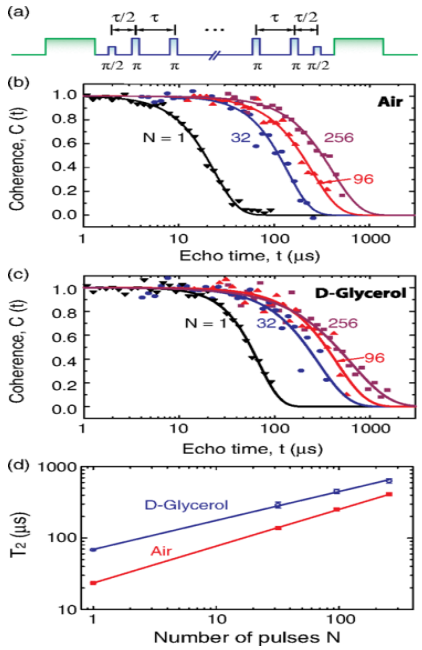

Fig. 12: Coherence echo times of NV center with and without the added d-glycerol with different pulse amounts. (M. Kim et. al.)

The coherence time measurements show an increase with pulse amount. The spectrum from the coherence data shows that it will fit an exponential function. Knowing the fit for the coherence data will allow the estimation of the frequency fluctuations which cause the decoherence.

The spectrum gained from the estimated frequency fluctuations will be the noise spectral density. The noise can be extracted using a spectral decomposition from the coherence time data.

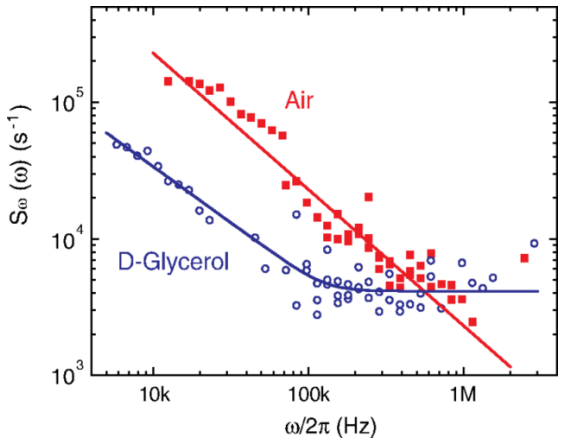

Fig. 13: Power spectral density of noise determined from spectral decomposition. (M. Kim et. al.)

Glycerol shows a good reduction in noise, but as the frequencies approach 1MHz the noise becomes worse than the lone NV center. There is a mechanism that is causing this reduction in noise when applying a protective layer. The dielectric constant is playing a role in how the noise is reduced. Possibilities for this deviation as frequencies reach 1MHz could be the following; the dielectric relaxation of glycerol is reducing at the surface of diamond, a nanometer thick layer of reduced mobility may be forming at the connecting interface, or thermal agitations of glycerol are becoming dominate.

Reduction of the dielectric relaxation of glycerol inherently considers the dielectric constant as being a frequency dependent parameter, it no longer acts as some real constant value. The dielectric relaxation has to do with the loss of the material. The dielectric loss of a material is related to the imaginary part of the frequency dependent dielectric constant. The mechanism that is causing this electric field noise for the near-surface NV center is still unknown.

There is an increase in coherence time with a protective layer, which leads to a reduction of the noise that causes decoherence and loss of sensitivity. A further understanding of this mechanism is much needed based off current published research.

Considered possibilities for the electric field surface noise never considered thermal noise as the major source. As the NV center is interacting with the environment thermal noise could be the culprit causing the major electric field noise. Looking at the protective layer system used in experimental research, the thermal noise can be modelled by using the fluctuation-dissipation theorem. The fluctuation dissipation theorem will allow the calculation of the charge noise spectral density due to electric field fluctuations from thermal noise.

Chapter 3

Model, Methodology, and Derivation

3.1 Protective Layer Model

Our model considers an NV center system near the surface of the crystal structure. In experiment these near surface NV centers are created by ^{15}N ion implantation [39,40]. This process places the NV center roughly 5nm from the surface. A protective layer is considered to be resting on top of the NV center surface. We are considering no chemical reactions take place when the protective layer is placed. This is warranted since the materials used are non-reactive and non-toxic. In current research, the created NV center diamond is also cleaned to get rid of any surface impurities. Also, other than DMSO, the materials are currently being used as protective layers in ongoing research.

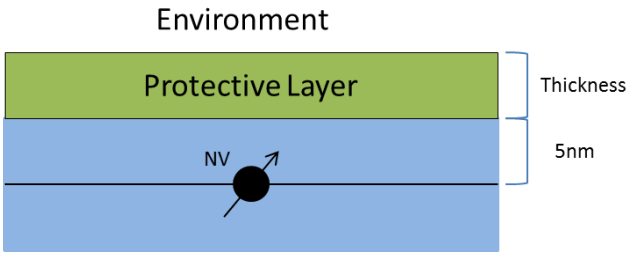

Fig. 14: NV center at 5nm depth with protective layer on top of certain thickness in an environment at room temperature.

From Fig. (14) there are two different lengths we need to consider; the depth of the NV center and the thickness of the protective layer. The environment is taken to be at constant room temperature.

We start our analysis by considering a monolayer system with the length of the protective layer being 5nm thick. This is not a practical model for use in experiment, but it allows us to eliminate a factor initially for analysis of the mechanisms determining the overall noise. The derivation of the thermal charge noise will take into account a monolayer system as well as a system for any value of the protective layer system. Throughout the analysis, we keep the depth of the NV the same value of 5nm.

3.2 Generalized Susceptibility

The energy can be defined by using the Hamiltonian operator. Working with interactions, my Hamiltonian will be split into two pieces. One piece will be the thermal equilibrium case with no external forces, while the other piece will deal with the interactions. The Hamiltonian is represented by,

$$H = H_0 + H_I(t). \qquad (4)$$

Here H_0 is the thermal equilibrium case, and $H_I(t)$ is the interaction case. We are considering a system that only depends on the electric field, so the magnetic field interactions, the zero field terms, and the bulk interactions of the Hamiltonian will be the thermal equilibrium piece. We can make this assumption due to in experiment, Hahn spin echo eliminates any thermal effect from these non-electric field interactions. The fluctuation-dissipation theorem requires my susceptibility to be in terms of correlation between charges,

$$\chi''(\boldsymbol{r}, t) = \frac{\langle [\hat{p}(\boldsymbol{r}, t), \hat{p}(\boldsymbol{r}', t')]_c \rangle_e}{2\hbar}. \qquad (5)$$

Here $\hat{p}$ is the electric dipole moment operator which is the ensemble of the total number (n) of electrons (e) and the total number (m) of nuclei (Z) at different locations (r). The electric dipole moment operator can be written in the following form,

$$\hat{p} = -e\sum_i^n r_i + -e\sum_j^m Z_j\, r_j. \qquad (6)$$

The interaction Hamiltonian can be directly related to the electric field and the electric dipole moment operator when considering electric dipolar interactions by,

$$H_I(t) = -\hat{p} * E(\boldsymbol{r}, t). \qquad (7)$$

Here $E(\boldsymbol{r}, t)$ is the applied electric field and $\hat{p}$ is the same electric dipole operator from before. To find the correlation between the electric dipole moment operators for the generalized susceptibility, we need to see how the Hamiltonian evolves with time. We begin by looking at the equation of motion for the density operator,

$$i\hbar\frac{d\rho(t)}{dt} = [H_0, \rho(t)] + [H_I(t), \rho(t)]. \qquad (8)$$

Here $\hbar$ is Planck's constant. The notion of equation of motion can be pictured as the change of the density operator in time, or also put the change in the density of states over time. Looking at the thermal equilibrium situation, we just have the first term in the sum,

$$i\hbar\frac{d\rho(t)}{dt} = [H_0, \rho(t)]. \qquad (9)$$

This differential equation will have the solution,

$$d\rho(t) = \frac{[H_0, \rho(t)]}{i\hbar}dt, \qquad (10)$$

$$\rho(t) = \rho_0 = \eta e^{\frac{-H_0}{k_B T}}. \qquad (11)$$

Here η is a normalization constant, k_B is Boltzmann's constant, and T is the temperature. The normalization constant (η) is set in such a way to allow for the trace of the density operator to be unity.

Now looking at the interaction piece of the equation of motion, we consider a perturbation series to obtain our solution. The perturbations on the density operator will be analogous to a mechanical spring oscillator under the influence of an electromagnetic field. The density operator is then written as,

$$\rho(t) = \rho_0(t) + \rho_1(t) + \ldots + \rho_n(t). \qquad (12)$$

Here the indices are the order of perturbation from the electric field ($\rho_{(n)}(t) \sim [E(t)]^{(n)}$) which go from 1 to n. Now to apply the boundary condition that at some time in the past the system was absent of external forces we have,

$$\rho(-\infty) = \rho_0. \qquad (13)$$

The perturbation series must be valid for all perturbations of the external electric field as time evolves. This will give us the boundary condition for our perturbation terms of the density operator,

$$\sum_{i=1}^{n} \rho_i(-\infty) = 0 \qquad i = 1,2,3,\ldots,n. \qquad (14)$$

We can now insert the perturbation series representation into the equation of motion. Our equation of motion then becomes,

$$i\hbar \frac{d(\rho_0(t) + \rho_1(t) + \ldots + \rho_n(t))}{dt} = [H_0, \rho_0(t) + \rho_1(t) + \ldots + \rho_n(t)] + [H_I(t), \rho_0(t) + \rho_1(t) + \ldots + \rho_n(t)]. \qquad (15)$$

Equating the terms with the same power dependence as the applied electric field on both sides, the following terms appear,

$$i\hbar\frac{d\rho_0(t)}{dt} = [H_0, \rho_0], \qquad (16)$$

$$i\hbar\frac{d\rho_1(t)}{dt} = [H_0, \rho_1(t)] + [H_I, \rho_0], \qquad (17)$$

$$i\hbar\frac{d\rho_2(t)}{dt} = [H_0, \rho_2(t)] + [H_I, \rho_1(t)], \qquad (18)$$

$$i\hbar\frac{d\rho_3(t)}{dt} = [H_0, \rho_3(t)] + [H_I, \rho_2(t)], \qquad (19)$$

$$\vdots$$

$$i\hbar\frac{d\rho_n(t)}{dt} = [H_0, \rho_n(t)] + [H_I, \rho_{n-1}(t)]. \qquad (20)$$

The first equation is our thermal equilibrium situation. The rest of the perturbation terms will then be consecutively solved from i = 1, 2, 3, …, n. To solve these equations, we want to look at how they evolve in time. The higher order terms will shrink much faster that the lower order terns, so when representing the system, we can just consider the n and n-1 terms.

To see how the density operator evolves in time, we can use the time evolution operator. The time evolution operator will need to work so that if left and right multiplied to the nth terms we get,

$$U(-t)\left\{i\hbar\frac{d\rho_n(t)}{dt} - [H, \rho_n(t)]\right\}U(t) = i\hbar\frac{d}{dt}\{U(-t)\rho_n(t)U(t)\}. \qquad (21)$$

First, we carry out the differentiation on the right-hand side using the chain rule,

$$i\hbar\frac{dU(-t)}{dt}\rho_n(t)U(t) + U(-t)i\hbar\frac{d\rho_n(t)}{dt}U(t) + U(-t)\rho_n(t)i\hbar\frac{dU(t)}{dt}. \qquad (22)$$

Expanding out the commutation on the left-hand side to get,

$$U(-t)\left\{i\hbar\frac{d\rho_n(t)}{dt} - H\rho(t) + \rho(t)H\right\}U(t). \qquad (23)$$

Finally, we do some manipulation and rearranging to get,

$$\left(i\hbar\frac{dU(-t)}{dt} + U(-t)H\right)\rho_n(t)U(t) + U(-t)\rho_n(t)\left(i\hbar\frac{dU(t)}{dt} - HU(t)\right) = 0. \qquad (24)$$

This statement is true if both bracket pieces are equal to zero. Setting each of them equal to zero,

$$i\hbar\frac{dU(-t)}{dt} + U(-t)H = 0, \qquad (25)$$

$$i\hbar\frac{dU(t)}{dt} - HU(t) = 0. \qquad (26)$$

These will have the following solutions,

$$U(t) = e^{-i\frac{H_0}{k_BT}}, \qquad (27)$$

$$U(-t) = e^{i\frac{H_0}{k_BT}}. \qquad (28)$$

We obtain the solutions for the time-evolution operator. These solutions can then be used along with two of their following properties,

$$U(t)U(t') = U(t+t'), \qquad (30)$$

$$U(t)U(-t) = U(0) = I. \qquad (31)$$

The time evolution operator has a two-time correlation and the corollary property which yields the identity matrix. Now we take the nth order equation of motion of the density operator and operating from the left with $U(-t)$ while operating from the right with $U(t)$,

$$i\hbar\frac{d}{dt}\big(U(-t)\rho_n(t)U(t)\big) = U(-t)[H_I, \rho_{n-1}(t)]U(t). \qquad (32)$$

Now integrating both sides we get,

$$U(-t)\rho_n(t)U(t) = \frac{1}{i\hbar}\int_{-\infty}^{t} U(-\tau)[H_I(\tau), \rho_{n-1}(\tau)]U(\tau)d\tau. \qquad (33)$$

The lower limit is fixed to satisfy our initial condition $\rho_n(-\infty) = 0$. Here τ is the time it takes to go from -∞ to an arbitrary time t. Now expanding the commutation and applying the operators and using their properties we obtain,

$$U(-t)\rho_n(t)U(t) = \frac{1}{i\hbar}\int_{-\infty}^{t} U(-\tau)[H_I(\tau)\rho_{n-1}(\tau) - \rho_{n-1}(\tau)H_I(\tau)]U(\tau)d\tau, \qquad (34)$$

$$" = \frac{1}{i\hbar}\int_{-\infty}^{t} U(-\tau)H_I(\tau)U(\tau)U(-\tau)\rho_{n-1}(\tau)U(\tau)$$

$$- U(-\tau)\rho_{n-1}(\tau)U(\tau)U(-\tau)H_I(\tau)U(\tau)d\tau, \qquad (35)$$

$$" = \frac{1}{i\hbar}\int_{-\infty}^{t} [U(-\tau)H_I(\tau)U(\tau), U(-\tau)\rho_{n-1}(\tau)U(\tau)]\, d\tau, \qquad (36)$$

$$Which\ gives, U(-t)H_I(t)U(t) = H_I{}'(t)\ and\ U(-t)\rho_{n-1}(t)U(t) = \rho'_{n-1}(t). \qquad (37)$$

We obtain time evolution transformations for the two equations of motion $H_I{}'(t)$ and $\rho'_n(t)$.

The inverse transformations are given by,

$$\rho_n(t) = U(t)\rho_n'(t)U(-t), \qquad (38)$$

$$H_I(t) = U(t)H_I{}'(t)U(-t). \qquad (39)$$

We use primed notation to denote that these are the time evolution transformations. Now using the relation between the interaction Hamiltonian and the electric dipole moment operator along with properties of the time-evolution operator, we gain the dynamics of the interaction Hamiltonian with respect to both space and time. Our primed notation Hamiltonian will become,

$$H_I{}'(\boldsymbol{r},t) = U'(\boldsymbol{r},t)[-\hat{p} * E(\boldsymbol{r},t)]U(\boldsymbol{r},t), \qquad (40)$$

$$H_I{}'(\boldsymbol{r},t) = U'(\boldsymbol{r},t)(-\hat{p})U(\boldsymbol{r},t)E(\boldsymbol{r},t), \qquad (41)$$

$$where\ U'(\boldsymbol{r},t) = U(\boldsymbol{r}',t') = U(-\boldsymbol{r},-t), \qquad (42)$$

$$H_I{}'(\boldsymbol{r},t) = -\hat{p}(\boldsymbol{r},t)E(\boldsymbol{r},t). \qquad (43)$$

We have the interaction Hamiltonian in terms of the electric dipole operator at a given position and time, but we still need to link the electric dipole operator to the generalized susceptibility we desire. To do this we can look at the definition of polarization and its relation to the electric susceptibility. The polarization density of a system is given by,

$$P(\boldsymbol{r},t) = \frac{\langle\hat{p}\rangle_e}{V}. \qquad (44)$$

From quantum mechanics, we can rewrite the expectation value in terms of the quantum mechanical trace. The polarization density is then rewritten as,

$$P(\boldsymbol{r},t) = \frac{Tr(\widehat{\rho_n}(\boldsymbol{r},t),\hat{p})}{V}. \qquad (45)$$

Next, we use the equation of motion for the density operator and use separation of variables. We integrate using our boundary condition that at some point in the past there is no external field. Our trace then becomes,

$$P(\boldsymbol{r},t) = \frac{1}{V} Tr\left[\left(U(\boldsymbol{r},t)\frac{1}{i\hbar}\int_{-\infty}^{t}[H_I{}'(\boldsymbol{r},\tau),\rho_{n-1}(\boldsymbol{r},\tau)]d\tau U'(\boldsymbol{r},t)\right),p\right], \quad (46)$$

$$Where\ \frac{1}{i\hbar}\int_{-\infty}^{t}[H_I{}'(\boldsymbol{r},\tau),\rho_{n-1}(\boldsymbol{r},\tau)]d\tau = \rho_n'(\boldsymbol{r},t), \quad (47)$$

$$and\ \left(U(\boldsymbol{r},t)\frac{1}{i\hbar}\int_{-\infty}^{t}[H_I{}'(\boldsymbol{r},\tau),\rho_{n-1}(\boldsymbol{r},\tau)]d\tau U'(\boldsymbol{r},t)\right) = \rho_n(\boldsymbol{r},t). \quad (48)$$

The interaction Hamiltonian can be rewritten in terms of the electric dipole moment operator and the electric field as seen before. The relation in terms of position and time dependence is given as,

$$[H_I{}'(\boldsymbol{r},\tau),\rho_{n-1}(\boldsymbol{r},\tau)] = [-\hat{p}(\boldsymbol{r},\tau)\cdot E(\boldsymbol{r},\tau),\hat{\rho}_{n-1}(\boldsymbol{r},\tau)] = -E(\boldsymbol{r},\tau)\,[\hat{p}(\boldsymbol{r},\tau),\hat{\rho}_{n-1}(\boldsymbol{r},\tau)]. \quad (49)$$

This is then plugged into our polarization density,

$$P(\boldsymbol{r},t) = \frac{1}{V} Tr\left(U(\boldsymbol{r},t)\frac{1}{i\hbar}\int_{-\infty}^{t} -E(\boldsymbol{r},\tau)\,[\hat{p}(\boldsymbol{r},\tau),\hat{\rho}_{n-1}(\boldsymbol{r},\tau)]d\tau U'(\boldsymbol{r},t)\,\hat{p}\right). \quad (50)$$

Now pulling the electric field and the integral out of the trace gives,

$$P(\boldsymbol{r},t) = -\frac{1}{i\hbar V}\int_{-\infty}^{t} E(\boldsymbol{r},\tau)\,Tr[U(\boldsymbol{r},t)[\hat{p}(\boldsymbol{r},\tau),\hat{\rho}_{n-1}(\boldsymbol{r},\tau)]U'(\boldsymbol{r},t)\hat{p}]\,d\tau. \quad (51)$$

The goal has been to determine a generalized electric susceptibility. We can now use the relationship between the polarization density and the electric susceptibility which is given by,

$$P(\boldsymbol{r},t) = \varepsilon_0\chi(\boldsymbol{r},t)E(\boldsymbol{r},t). \quad (52)$$

Plugging this into my polarization density equation and doing some manipulation, we obtain,

$$\varepsilon_0\chi(\boldsymbol{r},t)E(\boldsymbol{r},t) = -\frac{1}{i\hbar V}\int_{-\infty}^{t} E(\boldsymbol{r},\tau)\, Tr[U(\boldsymbol{r},t)[\hat{p}(\boldsymbol{r},\tau),\hat{\rho}_{n-1}(\boldsymbol{r},\tau)]U'(\boldsymbol{r},t)\hat{p}]\, d\tau, \qquad (53)$$

$$\chi(\boldsymbol{r},t) = -\frac{1}{i\varepsilon_0\hbar V}\int_{-\infty}^{t} Tr[U(\boldsymbol{r},t)[\hat{p}(\boldsymbol{r},\tau),\hat{\rho}_{n-1}(\boldsymbol{r},\tau)]U'(\boldsymbol{r},t)\hat{p}]\, d\tau. \qquad (54)$$

Focusing on the commutator and expanding it while applying the time-evolution operators, we have,

$$U(\boldsymbol{r},t)\hat{p}(\boldsymbol{r},\tau)U'(\boldsymbol{r},t)U(\boldsymbol{r},t)\hat{\rho}_{n-1}(\boldsymbol{r},\tau)U'(\boldsymbol{r},t) -$$
$$U(\boldsymbol{r},t)\hat{\rho}_{n-1}(\boldsymbol{r},\tau)U'(\boldsymbol{r},t)U(\boldsymbol{r},t)\hat{p}(\boldsymbol{r},\tau)U'(\boldsymbol{r},t). \qquad (55)$$

Using the properties of the time-evolution operator and simplifying to obtain,

$$U(\boldsymbol{r},t)[\hat{p}(\boldsymbol{r},\tau),\hat{\rho}_{n-1}(\boldsymbol{r},\tau)]U'(\boldsymbol{r},t) = [\hat{p}(\boldsymbol{r}'-\boldsymbol{r},\tau-t),\hat{\rho}_{n-1}(\boldsymbol{r},\tau)]. \qquad (56)$$

Plugging this into the equation for the electric susceptibility and using properties of the commutator, the equation becomes,

$$\chi(\boldsymbol{r},t) = -\frac{1}{i\varepsilon_0\hbar V}\int_{-\infty}^{t} Tr\big[\hat{\rho}_{n-1}(\boldsymbol{r},\tau)[\hat{p},\hat{p}(\boldsymbol{r}'-\boldsymbol{r},\tau-t)]\big]\, d\tau. \qquad (57)$$

The quantum mechanical trace is equivalent to the expectation value of the ensemble as indicated before. Using that definition and normalizing the system, we are able to get the generalized susceptibility as a correlation function. When using the fluctuation-dissipation theorem, the imaginary part of the susceptibility is what is used which will be explained later. That gives us,

$$\chi''(\boldsymbol{r},t) = \frac{\langle[\hat{p}(\boldsymbol{r},t),\hat{p}(\boldsymbol{r}',t')]_c\rangle_e}{2\hbar}. \qquad (58)$$

Here the notation $[\cdots]_c$ stands for the commutation, and $\langle\cdots\rangle_e$ stands for the expectation value of the ensemble. The prime notation for **r** and t are to denote a different independent set of position and time.

3.3 Thermal Charge Noise Density

With the generalized electric susceptibility, we can now use techniques to determine the thermal charge noise density. We begin by considering the Wiener-Khinchin theorem, which states that the autocorrelation function of a wide-sense stationary random process can be decomposed into a power spectrum for the process. The noise spectral density will be twice the Fourier transform of the correlation function of charge fluctuations [41]. The Wiener-Khinchin theorem is given by,

$$S(\boldsymbol{k},\omega) = 2\int_{-\infty}^{\infty} \chi_Q{}''(\boldsymbol{r},t;\boldsymbol{r}',t')\, e^{-i\omega t} dt. \qquad (59)$$

Here the subscript Q is to represent correlation between charges, $\boldsymbol{k}$ is the wave vector, and ω is the angular frequency. Doing the Fourier transform for the right-hand side, we obtain,

$$S(\boldsymbol{k},\omega) = 2\chi_Q{}''(\boldsymbol{k},\omega). \qquad (60)$$

Now we can introduce the fluctuation-dissipation theorem. The fluctuation-dissipation theorem predicts the behavior of thermal interactions at room temperature. This technique is a useful tool as it can apply to both classical and quantum mechanical systems. Plugging in our equation for the noise into the fluctuation-dissipation theorem, we obtain,

$$2\chi_Q{}''(\boldsymbol{k},\omega) = \frac{1-e^{-\frac{\hbar\omega}{k_B T}}}{\hbar}\int_{-\infty}^{\infty} \chi_Q{}''(\boldsymbol{r},t;\boldsymbol{r}',t')\, e^{-i\omega t} dt. \qquad (61)$$

Here k_B is Boltzmann's constant, and T is the temperature. The Fourier transform on the right-hand side is simply half of our Weiner-Khinchin theorem. Plugging in that fact gives,

$$2\chi_Q{}''(\boldsymbol{k},\omega) = \frac{1-e^{-\frac{\hbar\omega}{k_BT}}}{\hbar}\left(\frac{1}{2}S(\boldsymbol{k},\omega)\right). \qquad (62)$$

Doing some manipulation, the charge noise spectral density becomes,

$$S(\boldsymbol{k},\omega) = \frac{4\hbar}{1-e^{-\frac{\hbar\omega}{k_BT}}}\chi_Q{}''(\boldsymbol{k},\omega). \qquad (63)$$

Now considering the direction of the polarization density, the only major interactions will be along the polarization direction. For simplicity, we will set this direction to the z-axis. Only considering the polarization density along the interaction axis, we can rewrite the electric susceptibility. A direct relation comes out given by,

$$\chi_Q{}''(\boldsymbol{k},\omega) = \varepsilon_0 A^2 \chi_{P_z}{}''(\boldsymbol{k},\omega). \qquad (64)$$

Here ε_0 is the electric permittivity of free space, A is the area, and $\chi_{P_z}{}''(\boldsymbol{k},\omega)$ is the electric susceptibility along the interaction axis. Plugging this back into our noise equation, we obtain the following,

$$S(\boldsymbol{k},\omega) = \frac{4\hbar}{1-e^{-\frac{\hbar\omega}{k_BT}}}\varepsilon_0 A^2 \chi_{P_z}{}''(\boldsymbol{k},\omega). \qquad (65)$$

The noise equation is now dependent on two frequency dependent parameters, the electric permittivity and the electric susceptibility along the interaction axis. To make this equation more practical and useful with experimental values, we can rewrite this in terms of the dielectric loss tangent.

We start by looking at Ampere's law for matter,

$$\nabla \times \boldsymbol{H} = i\omega \boldsymbol{D} + \boldsymbol{J}_c, \qquad (66)$$

$$\nabla \times \boldsymbol{H} = i\omega\varepsilon \boldsymbol{E} + \sigma \boldsymbol{E}. \qquad (67)$$

Here $\boldsymbol{D}$ is the displacement field and $\boldsymbol{J}_c$ was the current density. Both have direct relations with the electric field, $\boldsymbol{D} = \varepsilon \boldsymbol{E}$ and $\boldsymbol{J}_c = \sigma \boldsymbol{E}$, where ε is the total electric permittivity and σ is the conductivity. Splitting the electric permittivity into its real (ε') and imaginary (ε'') parts and doing some manipulation, Ampere's law becomes,

$$\nabla \times \boldsymbol{H} = i\left[\omega\varepsilon' - i\left(\omega\varepsilon'' + \sigma\right)\right]\boldsymbol{E}. \qquad (68)$$

Looking just at the equation inside the brackets, we have the following,

$$\omega\varepsilon' - i\left(\omega\varepsilon'' + \sigma\right). \qquad (69)$$

Factoring out ω along with realizing $\left(\varepsilon'' + \frac{\sigma}{\omega}\right)$ is the total conductivity; we get a new equation for the total electric permittivity. This new representation relates the electric permittivity to the dielectric loss tangent and is given by,

$$\varepsilon = \varepsilon'(1 - itan\delta). \qquad (70)$$

The electric permittivity can also be written in terms of the relative permittivity (ε_r) and the permittivity of free space (ε_0),

$$\varepsilon = \varepsilon_0 \varepsilon_r, where\ \varepsilon_r = 1 + \chi. \qquad (71)$$

Now plugging these two different definitions my we get the following equation,

$$(1 + \chi)\varepsilon_0 = \varepsilon'(1 - itan\delta). \qquad (72)$$

The electric susceptibility can be split into its real and imaginary pieces. Making this change and doing some manipulation to obtain,

$$\chi'\varepsilon_0 + \varepsilon_0 - i\chi^{"}\varepsilon_0 = \varepsilon' - i\varepsilon' tan\delta. \qquad (73)$$

The fluctuation-dissipation considered the imaginary part of the susceptibility. This is due to looking at the imaginary pieces of the previous equation,

$$\varepsilon_0 \chi_{P_z}{}^{"}(\boldsymbol{k}, \omega) = \varepsilon'(\omega) tan\delta(\omega). \qquad (74)$$

Now we use the relation between the real part of the electric permittivity and the capacitance. The real permittivity will be directly related to the capacitance in the system,

$$\varepsilon'(\omega) = \frac{C(\omega)L}{A}. \qquad (75)$$

Here $C(\omega)$ is the frequency dependent capacitance, L is the thickness of the material, and A is the area. Doing some rearranging and manipulation, my electric susceptibility becomes,

$$\chi_{P_z}{}^{"}(\boldsymbol{k}, \omega) = \frac{C(\omega)L}{A\varepsilon_0} tan\delta(\omega). \qquad (76)$$

This can now be plugged into the noise equation to give,

$$S(\boldsymbol{k}, \omega) = \frac{4\hbar}{1 - e^{-\frac{\hbar\omega}{k_B T}}} C(\omega) LA tan\delta(\omega). \qquad (77)$$

There is one problem; the right-hand side only depends of frequency. We can fix this by considering the noise over the entire volume(V_0), where the volume will be $V_0 = AL$. Taking the noise over the entire volume, we obtain the entirely frequency dependent charge noise density,

$$S(\omega) = \frac{S(\boldsymbol{k},\omega)}{V_0} = \frac{4\hbar C(\omega)}{1 - e^{-\frac{\hbar\omega}{k_B T}}} tan\delta(\omega). \qquad (78)$$

3.4 Protective Layer System

The current thermal charge noise density equation is for a single material system without any protective layer. To answer the question of what mechanism is causing the reduction in noise, we have to consider the protective layer system. This will require me to take into account the capacitance and dielectric loss for both materials. First, we will look at the dielectric loss for a combined system. When considering the dielectric loss of both systems, they can be thought of as a superposition of the two dielectric losses [42-45]. Our relation for the dielectric loss for the protective layer system is then given by,

$$\phi_c = b_L d_L \phi_L + b_H d_H \phi_H. \qquad (79)$$

Here $b_{L,H}$ are the materials Young's modulus coefficients, $d_{L,H}$ is the materials thickness, and $\phi_{L,H}$ is the respective dielectric loss for the materials. The L and H stand for lower and higher index. These coefficients are given by,

$$b_{L,H} = \frac{1}{\sqrt{\pi} w}\left(\frac{Y_{L,H}}{Y_s} + \frac{Y_s}{Y_{L,H}}\right). \qquad (80)$$

The values $Y_{L,H}$ are the given materials Young's modulus, while Y_s is the surface Young's modulus. The value w is the width of the combination. With the new representation for the dielectric loss tangent, the thermal charge noise density has the following form,

$$S(\omega) = \frac{4\hbar C(\omega)}{1 - e^{-\frac{\hbar\omega}{k_B T}}} \phi_c. \qquad (81)$$

With the dielectric loss brought into the protective layer system, we can now look at the systems capacitance. Here capacitance is frequency dependent and we can relate it to the frequency dependent electric field as a plate capacitor,

$$C(\omega) = \frac{q}{E(\omega)L}. \qquad (82)$$

Here q is the charge, L is the thickness of the material, and $E(\omega)$ is the electric field. This electric field will simply be the Coulomb field [46],

$$E(\omega) = \frac{kq}{\varepsilon'(\omega)L^2}. \qquad (83)$$

Here k is the Coulomb law proportionality constant (k = $1/4\pi\varepsilon_0$). For the protective layer system, we have one layer of material on top of the other. The total capacitance will then be two capacitors in series. This will give an inverse addition to gain the overall capacitance and with some manipulation the total capacitance is,

$$C_{tot}(\omega) = \left(\frac{C_H + C_L}{C_H * C_L}\right)^{-1}. \qquad (84)$$

Both the capacitance and dielectric loss depend on the electric permittivity and are frequency dependent. The capacitance is directly proportional to the real part of the permittivity and the dielectric loss of a material is related to the ratio between the real and imaginary parts,

$$C(\omega) \propto \varepsilon'(\omega), \qquad (85)$$

$$tan\delta(\omega) = \frac{\varepsilon''(\omega)}{\varepsilon'(\omega)}. \qquad (86)$$

The frequency dependent permittivity that characterizes the capacitance and dielectric loss is a relaxation permittivity. The permittivity is given by the Havriliak-Negami relaxation [47]. This is a form of Debye permittivity given by,

$$\varepsilon(\omega) = \varepsilon_\infty + \frac{\Delta\varepsilon}{(1+(i\omega\tau)^\alpha)^\beta}. \qquad (87)$$

Here ε_∞ is the high frequency limit permittivity, $\Delta\varepsilon$ is the difference between the low limit and high limit, and τ is the characteristic relaxation time. The characteristic relaxation time is related to a materials relaxation frequency by $\tau = 1/2\pi f_r$, where f_r is the relaxation frequency. The exponents α and β describe the asymmetry (α) and the broadness (β) of the corresponding spectral density. The following table shows the material values used.

Material	Low Limit Permittivity	High Limit Permittivity	Relaxation Frequency	Young's/Bulk Modulus	Relaxation Time Constant	Alpha	Beta
NV Center Diamond	7.99	5.7	4.03E+05	443 GPa	2.48E-06	0.97	0.89
Glycerol	51.8	3.9	5.03E+07	4.8 GPa	1.99E-08	1	0.67
Propylene Carbonate (PC)	64.9	4.7	2.33E+10	8.0 GPa	4.30E-11	0.985	0.927
Dimethyl Sulfoxide (DMSO)	45.86	6.357	9.08E+09	4.5 GPa	1.10169E-10	1	1
Polymethyl Methacrylate (PMMA)	3.6	2.59	2.00E+05	5 GPa	0.000005	1	1
(microemulsions) Perfluoropolyether (PFPE)	104	10	1.43E+08	34.5 GPa	7.00E-09	0.87	1
Polyvinylidene Flouride (PVDF)	7.5	5	1.00E+04	1.1 GPa	0.0001	1	1

Table 1: Material properties for use with the Havriliak-Negami relaxation.

Chapter 4

Results and Discussions

4.1 Real and Imaginary Permittivity

Before fully analyzing the noise, some insight can be gained by looking at the graphs of the real and the imaginary parts of the permittivity. The imaginary part of the permittivity has a nonlinear relation with frequency compared to the real part (Fig. 15,16,17). The real part of the permittivity is mostly independent of frequency throughout the range $10^3 - 10^7$ Hz. Both glycerol and PFPE see changes in their real part of the permittivity approaching the high frequency region of the range analyzed. This change for glycerol and PFPE is from their permittivity beginning to become prominently imaginary. The imaginary part of the permittivity is attributed to loss in the system, while the real permittivity is the lossless part of the permittivity.

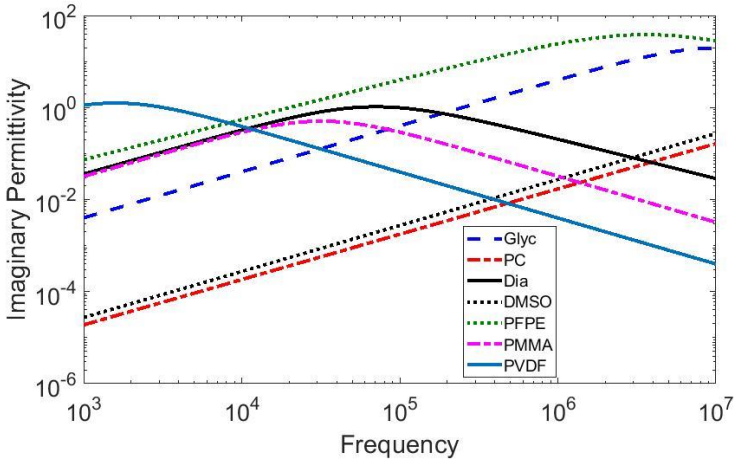

Fig. 15: Imaginary Permittivity vs. Frequency (log-log) of the lone diamond, liquids, and solids.

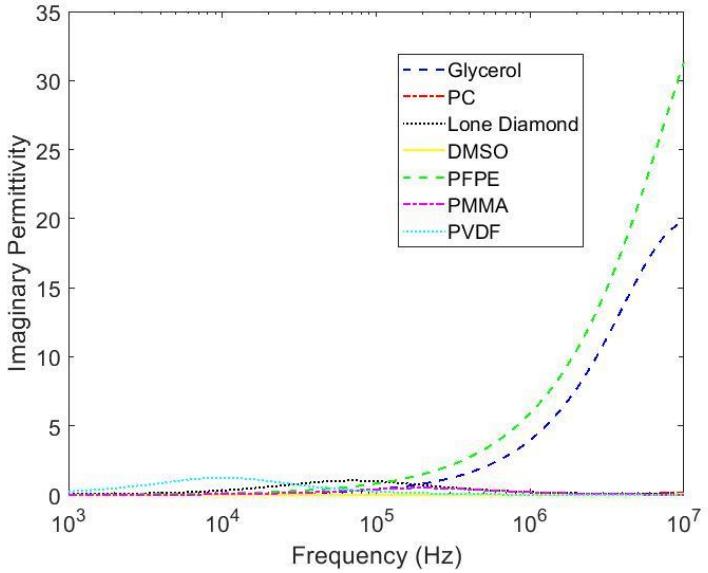

Fig. 16: Imaginary Permittivity vs. Frequency (semilog) of the lone diamond, liquids, and solids. The liquids are Glycerol, Propylene Carbonate, Dimethyl Sulfoxide, Perfluoropolyether. The solids are the Polyvinylidene Fluoride and Polymethyl Methacrylate.

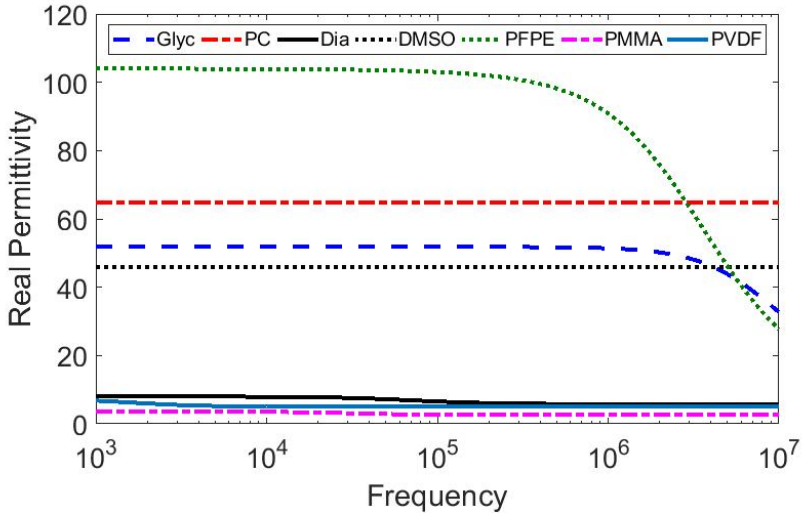

Fig. 17: Real Permittivity vs. Frequency of lone diamond, liquids and solids. The liquids are Glycerol, PC, DMSO, PFPE. The solids are the PVDF and PMMA.

Figure 17 and the equation for the capacitance (Eq. 82), which depends only on the real part of the permittivity, gives us some insight on how the capacitance will affect the noise. The capacitance should affect the noise by scaling it as another constant multiple for the system. Even with the change in glycerol and PFPE's real permittivity trend, at that point the imaginary permittivity will be dominating and shape the systems' noise. The imaginary part will dominate due to it being the loss piece of the permittivity in the system. Next, we graphed the capacitance and dielectric loss pieces of the system to see their dependence on frequency.

4.2 Capacitance and Dielectric Loss

The graphs of the capacitance and dielectric loss show that the dielectric loss tangent has a highly nonlinear trend (Fig. 18 and Fig. 19). Based off a total difference of 1×10^{-8} between the maximum and minimum of the capacitance for most of the systems, it undergoes negligible change and is independent of frequency as predicted. The dielectric loss shows a greater change over this range. For each of the systems, there is a steady increase initially. As the frequencies rise, the lone diamond, PC, PVDF, PMMA, and DMSO systems reach a peak in their dielectric losses then begin to fall. The glycerol and PFPE systems have a slight dip where the other systems peak, but they quickly turn back to a steady rising trend.

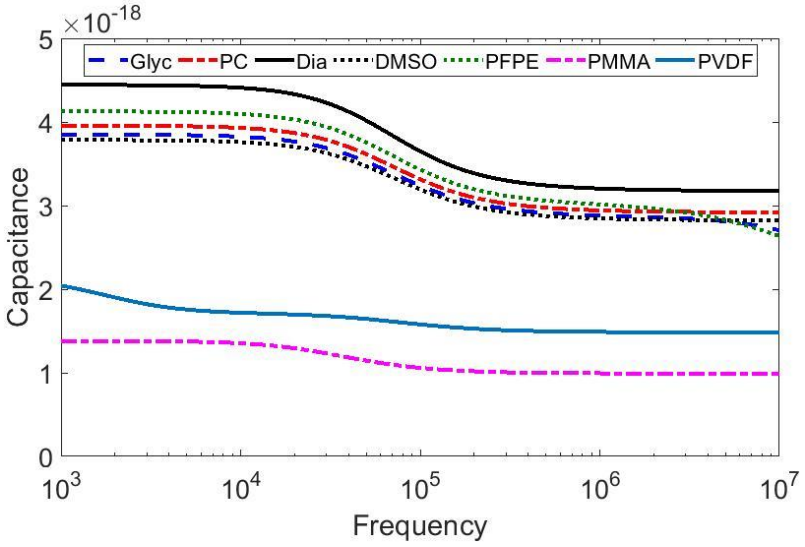

Fig. 18: Capacitance vs. Frequency. The lone diamond follows the single layer capacitance, while the others follow a series capacitance system.

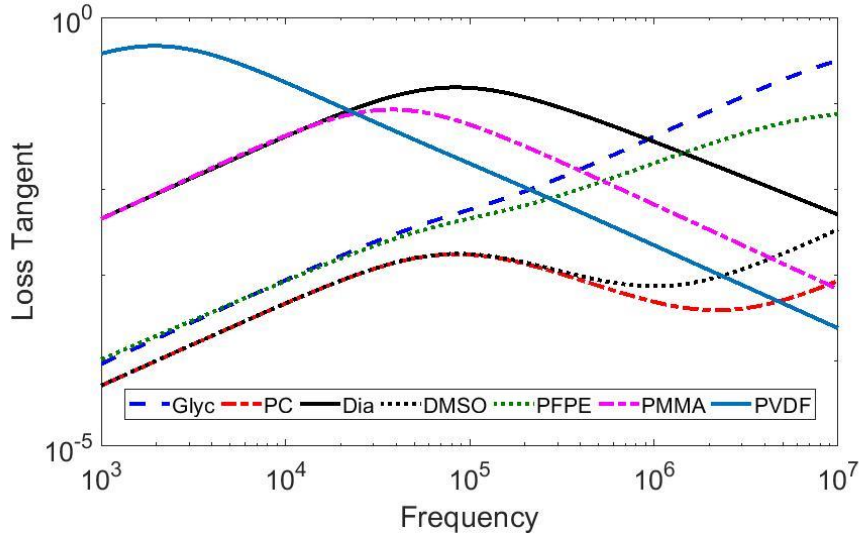

Fig. 19: Dielectric Loss vs. Frequency. The lone diamond is the usual ratio dielectric loss while the other systems take into account both materials dielectric loss.

These trends for the frequency dependent parameters show the dielectric loss has a greater effect on the noise than the capacitance. The capacitance acts more as a scaling constant. After determining the capacitance and the dielectric loss tangent, we analyzed the trend of the thermal charge noise spectrum.

4.3 Thermal Charge Noise Spectrum

At the lower frequencies the noise follows a white noise trend with the liquid protective layers giving a better reduction of the noise (Fig. 20). As frequencies increase, a power law reduction emerges. The lone diamond, PVDF, PMMA, and DMSO systems follow a power law ranging from $f^{-1.9} - f^{-2.2}$. For the propylene carbonate and PFPE systems, this power law is in the order of $f^{-1.6}$. Glycerol's system follows a much weaker power law compared to the rest on the order $f^{-0.5}$ which quickly levels out. The power laws for the lone diamond, PVDF, PMMA, PFPE, DMSO, and propylene carbonate systems are close to the order for Brownian noise which is of the order f^{-2}.

We also were able to observe that between 1 and 2 MHz lone diamond and the two solid protective layer systems crosses below glycerol. The noise for propylene carbonate and DMSO begins to flatten out at the 5 MHz frequency region. Fig. 5 also shows us different turning points in each of the noise spectra. For PVDF which gives the overall worse starting noise, its power law begins around 10^3 Hz. Lone diamond, glycerol, propylene carbonate, and PFPE all have a turning point at 4×10^4 Hz. All the liquid systems have a secondary turning point as frequencies reach the end of the spectrum.

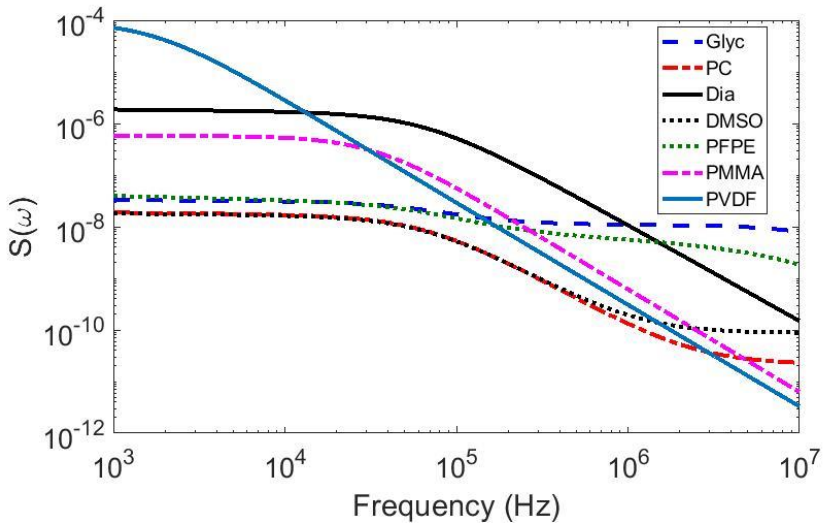

Fig. 20: Charge noise density spectrum. The lone diamond and the lone diamond with a solid protective layer start off worse than when a liquid protective layer is used.

To see what was causing these turning points, we took a closer look at the dielectric loss for each system. As the frequencies reach 4×10^4 Hz region for the dielectric loss, we see that this point corresponds to peaks for most of the systems (Fig 19). For glycerol and PFPE there is a small shrink in its rising trend at the same frequency region. The shrink is much less in glycerol than in PFPE. This peak for the lone diamond, PC, DMSO and the slight change in the glycerol and PFPE system corresponds to the turning point where the noise goes from white noise to the respective power laws. The peak of their dielectric losses corresponds to where the dielectric loss of the NV center peaks. Not just the protective layer's dielectric loss has a major effect on the noise of the system, but the NV centers' dielectric loss also has a prominent contribution. For PMMA and PVDF, Fig. 19 shows a different peak for the two systems. For PVDF this peak is at 10^3 Hz, where PMMA has a peak at 2×10^4 Hz.

Chapter 5

Analysis and Conclusions

5.1 Noise Trends and Dielectric Loss

The noise spectrum begins by following a white noise trend, but as the frequencies increase a power law trend like Brownian noise arises. For glycerol and PFPE, the power law trend is short lived compared to the others before they flatten out again. Glycerol also doesn't follow that strong its trend only reaching a power law of $f^{-0.5}$. For the other systems, their power laws are longer lived following power laws of $\approx f^{-1.6} - f^{-2.2}$. As the frequencies reach 0.4 to 1 MHZ, the noise for PVDF, PMMA and lone diamond drop below glycerol's noise respectively. In the region of 5 MHz, the noise for the propylene carbonate and DMSO systems begin to flatten out. Like the initial white noise trend of the noise spectrum, the flattening of glycerol, propylene carbonate, PFPE, and DMSO arises from their respective dielectric loss tangents.

The white noise trends come from the random interactions between the misaligned dipoles in the materials due to thermal noise. As the dielectric loss for a material peaks, a turning point arises, like seen with the initial turning point of the noise spectrum for each of the systems (Fig. 20).

This turning point in the noise for each of the materials happens at the point given by,

$$\frac{2\pi}{\tau_{eff}}, \quad (88)$$

$$where\ \tau_{eff} = \left(\frac{1}{\tau_{pro}} + \frac{1}{\tau_{NV}}\right)^{-1}. \quad (89)$$

Here τ_{eff} is the effective relaxation time and τ_{pro} and τ_{NV} are the relaxation times of the protective layer and the NV center respectively. For the liquid systems, the initial turning point is due to the first peak of the dielectric loss (Fig. 19). After this dielectric loss peaks, it begins to fall as the dipoles for a material have been able to realign and relax. The respective power laws for the systems come from the natural Brownian motion in the materials. For the solid systems, there is only one turning point which corresponds to their respective dielectric loss peaks (Fig. 19).

5.2 The Capacitance

The capacitance doesn't have a huge effect on the shape of the noise spectrum. Capacitance's contribution comes from how it scales down the noise of the system. Our systems are series capacitors, so the total capacitance will be lower than the lowest capacitor. The capacitance is directly related to the real permittivity for the material. We see that diamond by itself will have the highest capacitance as it has near the lowest real permittivity. Capacitance is acting as a constant in the system with its negligible dependence on frequency, but that does not mean the lowest capacitance will have the best starting noise. Figure 18 shows that the capacitances for the PDVF and PMMA systems are by far the lowest, but as they have a large rise in their dielectric loss at the low end of the spectrum their initial noise is much higher than the liquid systems.

5.3 The Physical Picture

Physically the system is losing electromagnetic energy due to thermal noise. This thermal noise misaligns the dipoles in the system. After being misaligned, the dipoles will start to interact with each other, giving off heat or other forms of radiation. Due to this process, a constant random noise, white noise, trend spectrum emerges. Eventually, enough time will pass for these dipoles to realign and their interactions will cease. This characteristic time constant for which the dipoles realign is the materials relaxation time, or in frequency space, their relaxation frequency.

The relaxation frequency from dipole relaxation will always be at the point where the dielectric loss for a given material will be maximum. The turning point in our charge noise spectrum is at these peaks for the dielectric loss for each system. The point at 10^5 Hz corresponds with the relaxation frequency of the NV center at room temperature. For the solid protective layer systems, the relaxation frequencies are close to the same order, so their peaks broaden and combine. This is shown by the PVDF having its peak at 10^3 Hz and PMMA having its peak at $3 \cdot 10^4$ Hz. As the dipoles relax and realign, the noise due to the interactions between them dissipates and the power law begins.

Quantum f^{-1} noise naturally appears and can be an important factor for overall noise [48]. Quantum noise arises from uncertainty in a physical property due to its quantum origin. Our system is working at room temperature and any major electric field noise will be due to thermal interactions. The quantum f^{-1} noise does not need to be considered for this system due to the strength of the thermal interactions. Thermal noise causing misaligned random dipole interactions and Brownian motion after relaxation are the main factors for the overall noise in the system.

5.4 Thickness Dependence

Throughout this we have considered a model with the thickness of the protective layer being the same as the depth of the NV center. This is not practical in experimental work as this would have the protective layer be 5nm thick. Most research has the liquid protective layer placed on with a pipette which will give a thickness on the order of a micron. Looking back at the final equation for noise, there are two terms that are dependent on the thickness of the materials; the capacitance and the dielectric loss. Plugging the equation for the electric field into the capacitance equation, we obtain,

$$C(\omega) = \frac{q}{\frac{kq}{\varepsilon' d^2} d}, \qquad (90)$$

$$C(\omega) = \frac{\varepsilon' d}{k}. \qquad (91)$$

Here ε' is the real permittivity, k is the Coulomb's law constant, and d is the thickness. The system we are studying has the capacitance as a pair of series capacitors. Plugging the single material capacitance into the total capacitance equation we will have the following,

$$C(\omega) = \frac{\frac{\varepsilon'_L d_L}{k} + \frac{\varepsilon'_H d_H}{k}}{\frac{\varepsilon'_L d_L \varepsilon'_H d_H}{k^2}}, \qquad (92)$$

$$C(\omega) = \frac{\varepsilon'_L d_L + \varepsilon'_H d_H}{\varepsilon'_L d_L \varepsilon'_H d_H} k. \qquad (93)$$

Here we denote the high and low index terms with H and L respectively. We already have the dielectric loss in terms of thickness. This allows us to now plug in my representation of the capacitance and the protective layer system dielectric loss into my equation for noise.

Encompassing the constants and all terms that do not depend on the thickness into an arbitrary function β we obtain,

$$S(\omega) = \beta\left(\frac{\varepsilon_L' d_L + \varepsilon_H' d_H}{\varepsilon_L' d_L \varepsilon_H' d_H}\right)(b_L d_L \phi_L + b_H d_H \phi_H). \qquad (94)$$

At this point the noise equation doesn't tell us much, but we can do some manipulation to get it into a more insightful form,

$$S(\omega) = \beta\left[\frac{\varepsilon_L' d_L^2 b_L \phi_L + \varepsilon_H' b_L d_L d_H \phi_L}{\varepsilon_L' d_L \varepsilon_H' d_H} + \frac{\varepsilon_L' b_H d_L d_H \phi_H + \varepsilon_H' b_H d_H^2 \phi_H}{\varepsilon_L' d_L \varepsilon_H' d_H}\right], \qquad (95)$$

$$S(\omega) = \beta\left[\left(\frac{\varepsilon_L' d_L^2 b_L + \varepsilon_H' b_L d_L d_H}{\varepsilon_L' d_L \varepsilon_H' d_H}\right)\phi_L + \left(\frac{\varepsilon_L' b_H d_L d_H + \varepsilon_H' b_H d_H^2}{\varepsilon_L' d_L \varepsilon_H' d_H}\right)\phi_H\right]. \qquad (96)$$

The noise is split into two terms, the noise dependent on the loss of the protective layer (ϕ_L) and the loss of the NV center (ϕ_H). The two terms have two pieces, the square of their own given thicknesses and the combination term.

We are considering now that the protective layer is 1μm ($\sim 10^{-6}$) and the NV center is at a depth of 1nm ($\sim 10^{-9}$). This allows for the noise to be simplified even further. Looking at the term dependent on the protective layer loss, there is a d_L^2 term and a combination $d_L d_H$ term. The d_L^2 term will be on the order of 10^{-12}, and $d_L d_H$ will be on the order of 10^{-15}. The squared term is three orders of magnitude larger than the combination term, allowing the cancelation of the combination term as it will be negligible in the sum. Similarly, the d_H^2 and $d_L d_H$ terms in the NV center loss dependent term, the d_H^2 term can be cancelled as it will be 4 orders of magnitude lower than the combination term.

This simplifies the noise equation to,

$$S(\omega) = \beta\left[\left(\frac{\varepsilon_L' d_L^2 b_L}{\varepsilon_L' d_L \varepsilon_H' d_H}\right)\phi_L + \left(\frac{\varepsilon_L' b_H d_L d_H}{\varepsilon_L' d_L \varepsilon_H' d_H}\right)\phi_H\right], \qquad (97)$$

$$S(\omega) = \beta\left[\frac{b_L}{\varepsilon_H'}\frac{d_L}{d_H}\phi_L + \frac{b_H}{\varepsilon_H'}\phi_H\right]. \qquad (98)$$

The new simplified noise equation shows us that our protective layer term will depend on both the frequency and the ratio of the thicknesses. Looking back at our graph of the imaginary permittivity and remembering the imaginary part of a materials permittivity is the major part of the loss, for solids and glycerol we see peaks and rises along with the NV center. For the liquids at the low frequencies, the imaginary part of their permittivity is negligible. Even PFPE doesn't really begin to rise until after the NV center has already peaked.

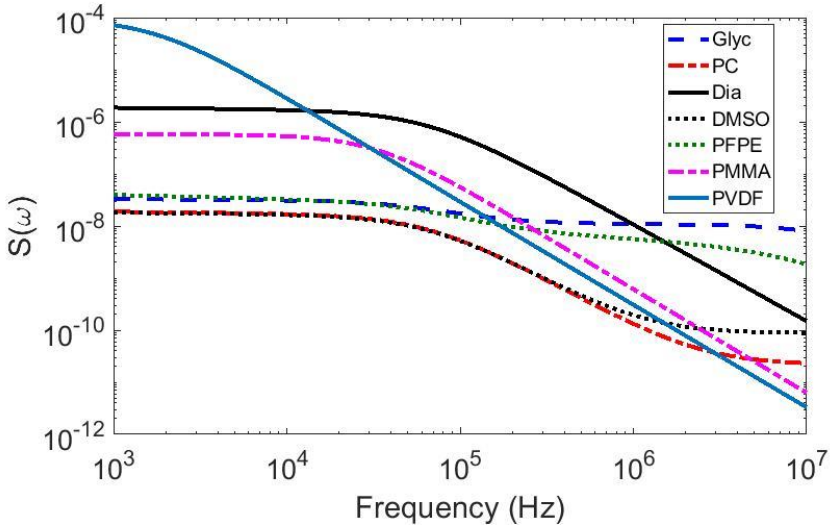

Fig. 20: Charge noise density spectrum with thickness and NV depth equal.

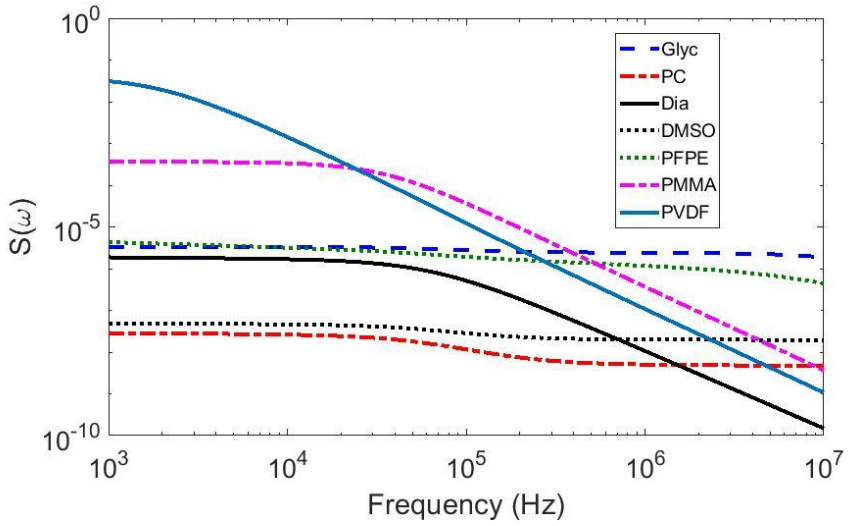

Fig. 21: Charge noise density spectrum with protective layer thickness at 1 micron.

Comparing the difference between the system with $d_L = d_H$ and the system with d_L= 1μm, we can see at low frequencies the thickness of the protective layer will act more as a constant multiple, and the shape of the noise will be dominated by the NV center term similar to before. At higher frequencies, the NV center term trends to zero, so the protective layer term takes over. With higher frequencies, the wavelength gets comparable to the material thickness. The shape of the noise at the higher frequencies will now be thickness dependent.

5.5 The Ideal System

The liquid systems have a much better noise throughout due to them having a much quicker (picosecond-nanosecond) relaxation time than solids do (microseconds). The quicker relaxation time comes from the liquids molecules being much more spread out while solids are much more compact. The spreading out of the dipoles allows their dipoles to realign much quicker. The solids having much more compact molecules allow the misaligned dipoles to interact much easier giving more surface noise. Following this same logic, gases would have the overall best reduction in noise, but this would not be a practical.

At low frequencies, the thickness of the protective layer does not play a major role on the shape of the noise spectrum. When the frequencies get to ranges where the wavelength is comparable to the thickness, the ratio between the protective layer system and the depth of the NV center becomes crucial. For solid protective layers and the glycerol protective layer, thickness is not a major factor in our studied range of frequencies. Both dielectric loss terms are rising at a similar rate for the solid protective layer and glycerol systems. Having a thicker solid or glycerol protective layer will give a worse starting point for the overall noise as the thickness is acting as a constant multiple; raising the capacitance and electric field for the material. With a liquid protective layer, at low frequencies the noise shape is dominated by the NV center term of the noise. As frequencies rise and the wavelength becomes comparable to the thickness, the loss of the liquids begins to peak and the ratio between lengths starts to affect the shape of the noise.

The most ideal system to protect the NV center from surface noise would be a material with a low real permittivity with a quick (picosecond range) relaxation time. The solid systems have a large dielectric loss early on due to both materials relaxation frequencies being near each other. With the misalignment of the dipoles in one material and then the beginning misalignment of dipoles in the other, the overall reduction in noise is much lower as frequencies increase. The dielectric loss is playing a major role in the protection of surface noise for these systems. Having a liquid top layer that has a large relaxation frequency for the dipole interactions with a small capacitance is the most practical way to protect the NV center from thermal surface noise.

5.6 Future Work

The work presented in this thesis investigated the surface noise due to electric field fluctuations from thermal interaction. This is just one piece of the total surface noise, as well as just one piece of the total noise.

Other surface effects that give rise noise can be studied to give the entire picture of the surface noise. Magnetic field surface noise has been known to be present for a while now and further study into this noise will add to the picture of the surface noise. The NV center is implanted 5nm deep, stress from underneath the NV center placement can also affect the surface noise. The surface effects are just part of the overall noise, the study of bulk noise is an important piece to understand.

The bulk of the material is a big factor is the noise of the system. The mechanisms of these bulk effects are not currently understood. The intuition of experimentalists has an idea on what bulk properties are causing the noise and decoherence in the NV center system, but a real understanding is not yet in place. When considering the bulk of diamond, the structure becomes important. The NV center has its own spin and is near a carbon atom which has its own spin. These spin-spin interactions can be a possible candidate for bulk noise. No diamond is 100% pure of a given isotope of carbon, a mix of carbon-12 and carbon-13 are littered throughout the material. The different carbon has different nuclear properties, such as carbon-13 has a higher probability of the electron being in the first excited state than in the ground state. This difference can cause for different nuclear spin effects, which can be another source of the bulk noise. Though stress could be another source of surface noise, it also can play a part in the bulk noise as well. The understanding of the bulk noise effects is vital to helping understand ways of reducing noise in the NV center system.

Bringing together the surface noise and bulk noise for the NV center, a better understanding of the system will arise. With this better understanding, ways of reducing the noise can be investigated in experiment.

After testing these theories of the noise, a clearer image can be seen by both the experimentalists and theorists. Refining the theory and experimental work can lead to the overall noise, surface and bulk, being solved.

References

[1] J.E. Graebner, *Thermal Conductivity of Diamond*, Springer, Boston, MA (1995).

[2] V. Danilenko, Physics of the Solid State **46**, 4, 595-599 (2004).

[3] B. Kharisov, Synthesis and Reactivity in Inorganic, Metal-Organic, and Nano-Metal Chemistry **40**, 84–101, (2010).

[4] Q. Zou, Materials Characterization **60**, 11, 1257-262 (2009).

[5] S. Felton, Physical Review B. **77,** 8, 081201. (2008)

[6] W. Doherty, B. Manson, P. Delaney, F. Jelezko, J. Wrachtrup, & L. C. Hollenberg, Physics Reports. **528** (1): 1–45 (2013)

[7] S. Choi, Physical Review B. **86** (4): 041202 (2012)

[8] L. Gordon, J. R. Weber, J. B. Varley, A. Janotti, D. D. Awschalom, & C. G. Van de Walle, MRS Bulletin. **38** (10): 802–807 (2013)

[9] L. J. Rogers, M. W. Doherty, M. S. J. Barson, S. Onoda, T. Ohshima, & N. B. Manson, New Journal of Physics. **17** (1): 013048 (2015)

[10] J. H. N. Loubser, & J. A. Van Wyk, Reports on Progress in Physics. **41** (8): 1201 (1978)

[11] G. Balasubramanian, I. Y. Chan, R. Kolesov, M. Al-Hmoud, J. Tissler, C. Shin, C. Kim, A. Wojcik, P. R. Hemmer, A. Krueger, T. Hanke, A. Leitenstorfer, R. Bratschitsch, F. Jelezko, & J. Wrachtrup, Nature **455**, 648-651 (2008)

[12] B. A. Myers, A. Ariyarante, & A. C. Bleszynski Jayich, Phys. Rev. Lett. **118**, 197201 (2017)

[13] M. Kim, H. J. Sherwood, K. Ohno, D. D. Awschalom, & D. Rugar, Phys. Rev. Lett. **115**, 087602 (2015)

[14] J. R. Maze, P. L. Stanwix, J.S. Hodges, S. Hong, J. M. Taylor, P. Cappellaro, L. Jiang, M. V. Gurudev Dutt, E. Togan, A. S. Zibrov, A. Yacoby, R. L. Walsworth, & M. D. Lukin, Nature **455**, 644-647 (2008)

[15] V. M. Acosta, E. Bauch, M. P. Ledbetter, C. Santori, K. M. C. Fu, E. Barclay, R. G. Beausolell, H. Linget, J. F. Roch, F. Treussart, S. Chemerisov, W. Gawlik, & D. Budker, Phys. Rev. B **80**, 115202 (2009)

[16] A. Jarmola, Z. Bodrog, P. Kehayias, M. Markham, J. Hall, D. J. Twitchen, V. M. Acosta, A. Gali, & D. Budker, Phys. Rev. B. **94**, 094108 (2016)

[17] F. Dolde, H. Fedder, M. W. Doherty, T. Nöbauer, F. Rempp, G. Balasubramanian, T. Wolf, F. Reinhard, L. C. Hollenberg, F. Jelezko, & J. Wrachtrup, Nature Physics **7**, 459 (2011)

[18] F. Dolde, M. W. Doherty, J. Michl, I. Jakobi, B. Naydenov, S. Pezzagna, J. Meijer, P. Neumann, F. Jelezko, N. B. Manson, & J. Wrachtrup, Phys. Rev. Lett. **111**, 227602 (2014)

[19] P. Ovartchaiyapong, K. W. Lee, B. A. Myers, & A. C. B. Jayich, Nat. Commun. **5**, 4429 (2014)

[20] E. R. MacQuarrie, T. A. Gosavi, N. R. Jungwritch, S. A. Bhave, & G. D. Fuchs, Phys. Rev. Lett. **111**, 227602 (2013)

[21] D. M. Toyli, C. F. de las Casas, D. J. Christle, V. V. Dobrovitski, & D. D. Awschalom, Proc. Natl. Acad. Sci. U.S.A. **110**, 8417 (2013)

[22] G. Kucsko, P. C. Maurer, N. Y. Yao, M. Kubo, H. J. Noh, P. K. Lo, H. Park, & M. D. Lukin, Nature (London) **500**, 54 (2013)

[23] M. S. Grinolds, S. Hong, P. Malentinsky, L. Luan, M. D. Lukin, R. L. Walsworth, & A. Yacoby, Nature Physics **9**, 215-219 (2013)

[24] T. Rosskopf, A. Dussaux, K. Ohashi, M. Loretz, R. Schiragl. H. Watanabe, S. Shikata, K. M. Itoh, & C. L. Degen, Phys. Rev. Lett. **112**, 147602 (2014)

[25] B. A. Myers, A. Das, M. C. Dartiailh, K. Ohno, D. D. Awschalom, & A. C. Bleszynski Jayich, Phys. Rev. Lett. **113**, 027602 (2014)

[26] Shigeru Ajisaka and Y. B. Band, Phys. Rev. B **94**, 134107 (2016)

[27] B. K. Ofori-Okai, S. Pezzanga, K. Chang, M. Loretz, R. Schirhagl, Y. Tao, B. A. Moores, K. Groot-Berning, J. Meijer, & C. L. Degen, Phys. Rev. B **86**, 081406 (2012)

[28] E. Togan, Y. Chu, A. S. Trifonov, L. Liang, J. Maze, L. Childress, M. V. G. Dutt, A. S. Sorensen, P. R. Hemmer, A. S. Zibrov, & M. D. Lukin, Nature **466**, 730-734 (2010).

[29] P. Neumann, N. Mizouchi, F. Rempp, P. Hemmer, H. Watanabe, S. Yamasaki, V. Jacques, T. Gaebel, F. Jelezko, & J. Wrachtrup, Science **320**, 1326 (2008)

[30] P. Neumann, R. Kolesov, B. Naydenov, J. Beck, F. Rempp, M. Steiner, V. Jacques, G. Balasubramanian, M. L. Markham, D. J. Twitchen, S. Pezzagna, J. Meijer, J.Twamley, F. Jelezko, & J. Wrachtrup, Nat. Phys. **6**, 249 (2010)

[31] P. Neumann, J. Beck, M. Steiner, F. Rempp, H. Fedder, P. R. Hemmer, J. Wrachtrup, & F. Jelezko, Science **329**, 542 (2010)

[32] G. Waldherr, J. Beck, M. Steiner, P. Neumann, A. Gali, Th. Frauenheim, F. Jelezko, & J. Wrachtrup, Phys. Rev. Lett. **106**, 157601 (2011)

[33] G. Waldherr, P. Neumann, S. F. Huelga, F. Jelezko, J. Wrachtrup, Phys. Rev. Lett. **107**, 129901 (2011)

[34] G. Balasubramanian, P. Neumann, D. Twitchen, M. Markham, R. Kolesov, N. Mitzuochi, J. Isoya, J. Achard, J. Beck, J. Tissler, V. Jacques, P. R. Hemmer, F. Jelezko, & J. Wrachtrup, Nat. Mater. 8, 383 (2009)

[35] P. Kehayais, A. Jarmola, N. Mosavain, I. Fescenko, F.M. Benito, A. Laraoui, J. Smits, L. Bougas, D. Budker, A. Neumann, S. R. J. Brueck & V. M. Acosta, Nature Communications **8**, 188 (2017)

[36] H. J. Mamin, M. Kim, M. H. Sherwood, C. T. Rettner, K. Ohno, D. D. Awschalom, & D. Rugar, Science **339**, 6119 (2013).

[37] D. B. Bucher, D. R. Glenn, J. Lee, M. D. Lukin, H. Park & R. L. Walsworth, arXiv:1705.08887 (2017).

[38] N. Aslam, M. Pfender, P. Neumann, R. Reuter, A. Zappe, F. F. Oliveira, A. Denisko, H. Sumiya, S. Onoda, J. Isoya & J. Wrachtrup, Science **7**, 357, 6346 (June 2017).

[39] M. Kim, H. J. Mamin, M. H. Sherwood, C. T. Rettner, J. Frommer, & D. Ruger, Appl. Phys. Lett. **105**, 042406 11 (2014).

[40] F. F´avaro de Oliveira, S. Momenzadeh, D. Antonov, H. Fedder, A. Denisenk, & J. Wrachtrup, Phys. Status Solidi, **8**, 2044-2050 (2016).

[41] M. Constantin, C. C. Yu, & J. M. Martinis, Physical Review B **79**, 094520 (2009)

[42] M. Principe, I. M. Pinto, V. Pierro, R. DeSalvo, & I. Taurasi, Physical Review D **91**, 022005 (2015)

[43] A. E. Villar, E. D. Black, R. DeSalvo, K. Libberecht, C. Michel, N. Morgado, L. Pinard, I. Pinto, V. Pierro, V. Galdi, M. Principe, & I. Taurasi Phys. Rev. D **81**, 122001 (2010).

[44] G. Harry, A. Gretarsson, P. Saulson, S. Kittelberger, S. Penn, W. Startin, S. Rowan, M. Fejer, D. R. M. Crooks, G. Cagnoli, J. Hough, & N. Nakagawa, Class. Quantum Grav. **19**, 897-917 (2002).

[45] G. Harry, H. Armandula, E. Black, D. R. M. Crooks, G. Cagnoli, J. Hough, P. Murray, S. Reid, S. Rowan, P. Sneddon, M. Fejer, R. Route, & S. Penn, App. Optics **45**, 7, 1569-1574 (2006).

[46] S. Havriliak & S. Negami, Polymer **8**, 161-210 (1967).

[47] J. D. Jackson, *Classical Electrodynamics* (Wiley, New York) (1975)

[48] P. Handel, Physical Review A **22**, 2 (1980)